



CREaTE

Canterbury Research and Theses Environment

Canterbury Christ Church University's repository of research outputs

<http://create.canterbury.ac.uk>

Please cite this publication as follows:

Zambetti, N., Ping, Z., Chen, S., Kenswill, K., Mylona, A., Sanders, M., Hoogenboezem, R., Bindels, E., Adisty, N., Van Strien, P., van der Leije, C., Westers, T., Cremers, E., Milanese, C., Mastroberardino, P., van Leeuwen, J., van der Eerden, B., Touw, I., Kuijpers, T., Kanaar, R., van der Loosdrecht, A., Vogl, T. and Raaijmakers, M. (2016) Mesenchymal inflammation drives genotoxic stress in hematopoietic stem cells and predicts disease evolution in human pre-leukemia. *Cell Stem Cell*, 19 (5). pp. 613-627. ISSN 1934-5909.

Link to official URL (if available):

<https://doi.org/10.1016/j.stem.2016.08.021>

This version is made available in accordance with publishers' policies. All material made available by CReaTE is protected by intellectual property law, including copyright law. Any use made of the contents should comply with the relevant law.

Contact: create.library@canterbury.ac.uk



Cell Stem Cell

Oncogenic niche signaling in human leukemia predisposition syndromes

--Manuscript Draft--

Manuscript Number:	CELL-STEM-CELL-D-15-00707R1
Full Title:	Oncogenic niche signaling in human leukemia predisposition syndromes
Article Type:	Research Article
Keywords:	hematopoietic stem cell; hematopoietic stem cell niche; leukemia; inflammation; DNA damage.
Corresponding Author:	Marc Raaijmakers Erasmus Medical Center Cancer Institute Rotterdam, NETHERLANDS
First Author:	Noemi A. Zambetti
Order of Authors:	Noemi A. Zambetti Zhen Ping Si Chen Keane J. G. Kenswil Maria A. Mylona Mathijs A. Sanders Remco M. Hoogenboezem Eric M. J. Bindels Maria N. Adisty Paulina M. H. Van Strien Cindy S. van der Leije Theresia M. Westers Eline M. P. Cremers Chiara Milanese Pier G. Mastroberardino Johannes P. T. M. van Leeuwen Bram C. J. van der Eerden Ivo P. Touw Taco W. Kuijpers Roland Kanaar Arjan A. van de Loosdrecht Thomas Vogl Marc H. G. P. Raaijmakers
Abstract:	Mesenchymal niche cells may drive tissue failure and malignant transformation in the hematopoietic system but the molecular mechanisms and their relevance to human disease remain poorly defined. Here, we show that perturbation of mesenchymal cells in a mouse model of the preleukemic disorder Shwachman-Diamond syndrome induces mitochondrial dysfunction, oxidative stress and activation of DNA damage responses in hematopoietic stem and progenitor cells. Massive parallel RNA sequencing of highly purified mesenchymal cells in the mouse model and a range of human preleukemic syndromes identified p53-S100A8/9-TLR inflammatory signaling as a common driving mechanism of genotoxic stress.

Transcriptional activation of this signaling axis in the mesenchymal niche predicted leukemic evolution and progression-free survival in myelodysplastic syndrome, the principal leukemia predisposition syndrome. Collectively, our findings reveal a concept of mesenchymal niche-induced genotoxic stress in heterotypic stem and progenitor cells through inflammatory signaling as an actionable determinant of disease outcome in human preleukemia.

Oncogenic niche signaling in human leukemia predisposition syndromes.

Noemi A. Zambetti^{1,8}, Zhen Ping^{1,8}, Si Chen^{1,8}, Keane J. G. Kenswil¹, Maria A. Mylona¹, Mathijs A. Sanders¹, Remco M. Hoogenboezem¹, Eric M. J. Bindels¹, Maria N. Adisty¹, Paulina M. H. Van Strien¹, Cindy S. van der Leije², Theresia M. Westers³, Eline M. P. Cremers³, Chiara Milanese⁴, Pier G. Mastroberardino⁴, Johannes P. T. M. van Leeuwen², Bram C. J. van der Eerden², Ivo P. Touw¹, Taco W. Kuijpers⁵, Roland Kanaar⁶, Arjan A. van de Loosdrecht³, Thomas Vogl⁷ and Marc H. G. P. Raaijmakers^{1,*}.

¹Department of Hematology, Erasmus MC Cancer Institute, Rotterdam 3015CN, The Netherlands

²Department of Internal Medicine, Erasmus MC Cancer Institute, Rotterdam 3015CN, The Netherlands

³Department of Hematology, VU University Medical Center, Cancer Center Amsterdam, Amsterdam 1081HV, The Netherlands

⁴Department of Molecular Genetics, Erasmus MC Cancer Institute, Rotterdam 3015CN, The Netherlands

⁵Department of Pediatric Hematology, Immunology and Infectious Diseases, Emma Children's Hospital, Academic Medical Centre (AMC), University of Amsterdam (UvA), Amsterdam 1105AZ, The Netherlands

⁶Department of Genetics, Cancer Genomics Center, Department of Radiation Oncology, Erasmus MC Cancer Institute, Rotterdam 3015CN, The Netherlands

⁷Institute of Immunology, University of Münster, Münster 48149, Germany

⁸Co-first author

*Correspondence: m.h.g.raaijmakers@erasmusmc.nl

HIGHLIGHTS

1. Mesenchymal niche cells induce genotoxic stress in HSPCs in a mouse model of SDS
2. p53-S100A8/9-TLR4 inflammatory signaling is identified as the underlying mechanism
3. Mesenchymal S100A8/9 predicts leukemic evolution and disease outcome in MDS

SUMMARY

Mesenchymal niche cells may drive tissue failure and malignant transformation in the hematopoietic system but the molecular mechanisms and their relevance to human disease remain poorly defined. Here, we show that perturbation of mesenchymal cells in a mouse model of the preleukemic disorder Shwachman-Diamond syndrome induces mitochondrial dysfunction, oxidative stress and activation of DNA damage responses in hematopoietic stem and progenitor cells. Massive parallel RNA sequencing of highly purified mesenchymal cells in the mouse model and a range of human preleukemic syndromes identified p53-S100A8/9-TLR inflammatory signaling as a common driving mechanism of genotoxic stress.

Transcriptional activation of this signaling axis in the mesenchymal niche predicted leukemic evolution and progression-free survival in myelodysplastic syndrome, the principal leukemia predisposition syndrome. Collectively, our findings reveal a concept of mesenchymal niche-induced genotoxic stress in heterotypic stem and progenitor cells through inflammatory signaling as an actionable determinant of disease outcome in human preleukemia.

INTRODUCTION

Genotoxic stress results in the accumulation of DNA lesions in hematopoietic stem and progenitor cells (HSPCs) over the lifespan of an organism, contributing to tissue failure and malignant transformation (Jaiswal et al., 2014; Rossi et al., 2007). The pathophysiological insults underlying genomic stress in HSPCs, however, remain incompletely understood. Perturbed signaling from their surrounding microenvironment may be implicated, but this has not been experimentally defined.

Components of the bone marrow microenvironment have emerged as key regulators of normal and malignant hematopoiesis (Arranz et al., 2014; Hanoun et al., 2014; Medyouf et al., 2014; Schepers et al., 2015; Walkley et al., 2007). We, and others, have shown that primary alterations of the mesenchymal niche can induce myelodysplasia and promote the emergence of acute myeloid leukemia (AML) with cytogenetic abnormalities in HSPCs (Kode et al., 2014; Raaijmakers et al., 2010), thus introducing a concept of niche-driven oncogenesis in the hematopoietic system.

To provide insights into the mechanisms that underlie this concept, as well as their relevance for human disease, we modeled the human leukemia predisposition disorder Shwachman-Diamond syndrome (SDS), caused by constitutive homozygous or compound heterozygous loss of function mutations in the *SBDS* gene, required for ribosome biogenesis (Boocock et al., 2003; Finch et al., 2011). SDS is characterized by skeletal defects in conjunction with a striking propensity to develop myelodysplastic syndrome (MDS) and AML at a young age, with a cumulative probability of >30% at the age of 30 years and a median onset at 18 years (Alter, 2007; Donadieu et al., 2012). Hematopoietic cell intrinsic loss of *Sbds* does not result in MDS or leukemia (Rawls et al., 2007; Zambetti et al., 2015), supporting the notion that cell-extrinsic factors contribute to malignant transformation. Deletion of *Sbds* from mesenchymal cells expressing the mesenchymal progenitor marker osterix (*Sp7*) in the bone marrow induced apoptosis in HSPCs and myelodysplasia, but the molecular mechanisms driving these observations and their relevance for human disease remained to be defined (Raaijmakers et al., 2010).

Here, we identify the endogenous damage-associated molecular pattern (DAMP) molecules S100A8 and S100A9, secreted from mesenchymal niche cells, as drivers of mitochondrial dysfunction, oxidative stress and DNA damage response (DDR) activation in HSPCs, with clinical relevance to the pathogenesis and prognosis of human bone marrow failure and leukemia predisposition syndromes.

RESULTS

Deletion of *Sbds* from mesenchymal progenitor cells (MPCs) recapitulates skeletal abnormalities of human SDS

SDS is characterized by bone abnormalities including low-turnover osteoporosis with reduced trabecular bone volume, low numbers of osteoblasts, and reduced amount of osteoid, leading to increased risk of fractures (Toiviainen-Salo et al., 2007). The cellular subsets driving these abnormalities and the underlying molecular mechanisms have remained largely undefined. We have previously shown that Cre-mediated deletion of *Sbds* from osterix⁺ MPCs (*Sbds*^{ff} *Osx*^{cre/+} mice, hereafter OCS^{ff} or mutants) disrupts the architecture of the marrow and cortical bone (Raaijmakers et al., 2010). Here, we first sought to better define the skeletal defects in these mice and their relevance to human disease.

OCS^{ff} mice presented growth retardation and reduced femur length compared to control *Sbds*^{f/+} *Osx*^{cre/+} (OCS^{f/+}) mice (Figure 1A and 1B) as observed in human patients (Aggett et al., 1980; Ginzberg et al., 1999). The runted phenotype was associated with a significantly limited lifespan, with lethality observed after the age of 4 weeks. Analyses were therefore performed in three week-old mice. The femur trabecular area was profoundly reduced in OCS^{ff} mice, with decreased bone volume, low number of trabeculae, increased trabecular spacing and reduced numbers of osteoblasts compared to controls (Figure 1C-1G, and 1I). The cortical bone of OCS mutants was also affected, as indicated by low bone mineral density values (Figure 1C-1D and 1H), attenuating the mechanical

properties of the bone, which was found less resistant to fracture in three-point bending test (Figure 1J). A tendency for reduced stiffness in the long bones was also observed (Figure 1K). Taken together, the structural and mechanical defects indicate that *Sbds* deficiency in MPCs causes osteoporosis with a propensity for fracturing, in line with observations in SDS patients (Ginzberg et al., 1999; Mäkitie et al., 2004; Toiviainen-Salo et al., 2007). Impaired osteogenesis did not reflect a contraction of the bone progenitor cell pool as shown by frequency of CFU-F and *Osx::GFP*⁺ cells (Figure S1A and S1B), but rather impairment of terminal osteogenic differentiation as suggested by transcriptional profiling of prospectively isolated osterix-expressing (*GFP*⁺) cells (Figure S1C). Transcriptional data confirmed deregulated expression of genes related to ribosomal biogenesis and translation (Figure S1D and S1E), in line with the established role of *Sbds* in ribosome biogenesis. Collectively, this data supports a view in which bone abnormalities in SDS are caused by deficiency of *Sbds* in MPCs, which attenuates terminal differentiation towards matrix-depositing osteoblastic cells with a compensatory increase in the most primitive mesenchymal compartment.

***Sbds* deficiency in the hematopoietic niche induces mitochondrial dysfunction, oxidative stress and activation of the DNA damage response in HSPCs**

Having established that the OCS mice represent a *bona fide* model for bone abnormalities in human disease, we next investigated the hematopoietic consequences of these environmental alterations. HSPC number was unaltered in OCS mice (Figure S2A-S2C) and HSPCs displayed global preservation of their transcriptional landscape after exposure to the *Sbds*-deficient environment (Figure S2D-S2F). Transcriptional network analysis, however, revealed significant overlap with signatures previously defined as predicting leukemic evolution of human CD34⁺ cells (Li et al., 2011), including pathways signaling mitochondrial abnormalities (Figure 2A; Table S1). Mitochondrial dysfunction was confirmed by measuring the mitochondrial membrane potential ($\Delta\psi$), indicating hyperpolarization of the mitochondria (Figure 2B and 2C). Mitochondrial hyperpolarization can result in reverse electron transfer, leading to the production of superoxide radicals, which can be

further converted into other reactive oxygen species (ROS) (Murphy, 2009). In line with this, a marked increase in intracellular ROS levels was found in OCS mutant HSPCs (Figure 2D), more specifically superoxide radicals derived from mitochondria as shown by dihydroethidium (DHE) staining (Figure S2G) (Owusu-Ansah et al., 2008; Stowe et al., 2009). ROS can undermine the genomic integrity of HSPCs by inducing DNA damage (Ito et al., 2006; Walter et al., 2015; Yahata et al., 2011), to which normal HSPCs react by activating the DDR and DNA repair pathways (Rossi et al., 2007). Indeed, HSPCs (LKS-SLAM) cells from OCS^{f/f} mice displayed accumulation of Ser139-phosphorylated H2AX histone (γ H2AX), which forms at the sites of DNA damage (Figure 2E; Figure S2H). Treatment of OCS mutant animals with the ROS scavenger N-acetylcysteine (NAC) resulted in partial reduction in the accumulation of γ H2AX (Figure S2I and S2J). Congruent with genotoxic effects of the mutant microenvironment, HSPCs displayed transcriptional modulation of DDR and DNA repair pathways (Table S2), including nucleotide excision repair programs, associated with ROS-induced lesions (Curtin, 2012) and signatures related to the master regulator of DDR and cell checkpoint activation ataxia telangiectasia and Rad3-related (ATR). Activation of the G1-S cell cycle checkpoint, resulting in cell cycle arrest, was suggested by depletion of S-phase transcriptional signatures (Figure 2F; Table S1), *in vivo* BrdU/Ki67 labeling (Figure 2G and 2H; Figure S2K) and downregulation of the Myc pathway, a critical regulator for this restriction point and the coordination of S–G2–M progression (Figure 2I; Table S3). Apoptosis of mutant HSPCs, as an alternative outcome of checkpoint activation, was earlier demonstrated (Raaijmakers et al., 2010). Together, the data indicate that the *Sbds*-deficient environment induces mitochondrial dysfunction, oxidative stress, DNA damage and genotoxic stress in HSPCs leading to activation of DDR pathways and G1-S checkpoint activation, reminiscent of a model in which mitochondrial dysfunction underlies an escalating cycle of increased ROS and genotoxic damage (Sahin and Depinho, 2010).

Short term exposure to the genotoxic environment did not attenuate HSPC function in DNA repair proficient cells, as demonstrated by competitive transplantation experiments (Figure S3A-S3C),

suggesting efficient DNA-repair or elimination of functionally impaired HSPCs by the DDR-driven apoptosis and cell cycle arrest. Congruent with this notion, alkaline comet assays on sorted HSPCs failed to demonstrate structural DNA damage (Figure S3D and S3E).

Activation of the p53 pathway drives bone abnormalities and genotoxic stress in OCS mice

Next, we sought to define the molecular programs underlying the bone and hematopoietic alterations in OCS mice. A proposed common molecular mechanism for the pathogenesis of ribosomopathies involves activation of the p53 tumor suppressor pathway (Raiser et al., 2014). The p53 protein was overexpressed in GFP⁺ MPCs in OCS mutants, with activation of downstream transcriptional pathways and upregulation of canonical targets (Figure 3A-3C). To assess the pathophysiological role of p53 activation in MPCs, we intercrossed OCS with *Trp53*-floxed mice (Marino et al., 2000), generating a double conditional knock-out model where the deletion of p53 is localized in the *Sbds*-deleted stromal compartment (*Sbds*^{f/f} *Trp53*^{f/f} *Osx*^{cre/+} mice; hence OCS^{f/f} p53^Δ) (Figure 3D). Genetic recombination of the *Trp53* locus was detected only in bone cells-containing samples, demonstrating the tissue specificity of p53 deletion in this model (Figure 3E). Genetic deletion of p53 from *Sbds*-deficient MPCs rescued the osteoporotic phenotype (Figure 3F-3J), but not cortical bone mineralization (Figure 3K), while it had only modest effects on bone mass in OCS control mice (Figure S4), in line with earlier observations (Wang et al., 2006). Rescue of the skeletal phenotype was linked to amelioration of genotoxic stress in HSPCs as demonstrated by a reduction of superoxide radicals derived from mitochondria and DNA damage (Figure 3L and 3M).

Identification of the damage-associated molecular pattern genes *S100A8* and *S100A9* as candidate niche factors driving genotoxic stress in human leukemia predisposition syndromes

To identify human disease-relevant niche factors, downstream of p53 activation, driving genomic stress in HSPCs, we compared the transcriptomes of GFP⁺ MPCs from OCS mice to those from prospectively FACS-isolated mesenchymal CD271⁺ niche cells (Tormin et al., 2011) from human

SDS patients (Figure 4A; Table S4). The mesenchymal nature of CD271⁺ cells was confirmed by CFU-F capacity and differential expression of mesenchymal, osteolineage and HSPC-regulatory genes (Chen et al, 2016). RNA sequencing showed the presence of *SBDS* mutations (Figure 4B; Figure S5; Table S4) associated with reduced *SBDS* expression (Figure 4C), confirming molecular aspects of SDS in previous studies (Finch et al., 2011; Woloszynek et al., 2004). Identical transcriptional signatures of disrupted ribosome biogenesis and translation were found in human niche cells (Figure 4D) and in GFP⁺ cells from OCS mice (Figure S1E), confirming faithful recapitulation of human molecular disease characteristics in the mouse model. Forty genes were differentially expressed both in the mouse model and human SDS, 25 of which were overexpressed, with a remarkable abundance of genes encoding proteins implicated in inflammation and innate immunity (Figure 4E).

To further delineate candidate genes driving genomic stress and leukemic evolution from this gene set, we performed whole transcriptome sequencing of CD271⁺ cells in two related human bone marrow failure and leukemia predisposition disorders: (1) low-risk MDS, the principal human preleukemic disorder in which cell cycle exit (senescence), accumulation of ROS, DNA damage and apoptosis have been described (Head et al., 2011; Peddie et al., 1997; Xiao et al., 2013), reminiscent of HSPC phenotypes in OCS mice, and (2) DBA, like SDS, a ribosomopathy characterized by bone marrow failure, but with a much lower propensity to evolve into AML (<1% with longer latency than observed in SDS and MDS) (Vlachos et al., 2012) (Table S4). We reasoned that genes specifically overexpressed in mesenchymal niche cells from disorders with as strong propensity for leukemic evolution (SDS and MDS) might represent strong candidate drivers of genotoxic stress. Eleven such genes were found (Figure 4F), among which the damage-associated molecular pattern (DAMP) *S100A8* and *S100A9*, significantly ($P<0.05$) differentially expressed in GFP⁺ cells from OCS mutant mice (Figure 4E-4G) and a *bona fide* downstream transcriptional target of p53 (Li et al., 2009). Ex

vivo shRNA experiments confirmed that upregulation of both p53 and S100A8/9 are direct, cell-intrinsic consequences of *Sbds* downregulation in mesenchymal precursor (OP9) cells (Figure S6A).

Niche-derived S100A8/9 induces genotoxic stress in murine and human HSPCs

S100A8 and *S100A9* belong to a subclass of proinflammatory molecules referred to as DAMP or alarmins. DAMPs are endogenous danger signals that are passively released or actively secreted in the microenvironment after cell death, damage or stress and bind pattern recognition receptors (PRR) to regulate inflammation and tissue repair (Srikrishna and Freeze, 2009). S100A8 and S100A9 proteins were overexpressed in mouse *Sbds*-deficient MPCs (Figure 5A and 5B) and increased plasma concentration of S100A8/9 indicated secretion of the heterodimer (Figure 5C). Its canonical receptor TLR4 (Vogl et al., 2007) is expressed in murine HSPCs (Figure S6B) and the canonical downstream signaling NF- κ B and MAPK pathways were activated in HSPCs from OCS^{f/f} mice (Figure S6C).

Exposure of HSPCs (LKS) cells to recombinant murine S100A8/9 resulted in increased DNA damage (number of γ H2AX and 53BP1 foci) (Figure 5D; Figure S6D), which was replication-independent (Figure 5E), and apoptosis (Figure 5F), associated with activation of TLR signaling (Figure 5G; Table S5), recapitulating the *in vivo* HSPC phenotype (Raaijmakers et al., 2010). *In vivo*, blockage of TLR4 by neutralizing antibodies resulted in a reduction of γ H2AX foci in LKS cells from OCS^{f/f} mice (Figure 5H).

To provide formal experimental support for the view that S100A8/9 production by ancillary cells in the bone marrow microenvironment is sufficient to drive genotoxic stress in HSPCs in a paracrine manner, we next transplanted CD45.1⁺ wild type hematopoietic cells into S100A9-GFP transgenic (S100A9Tg) mice, overexpressing both *S100A8* and *S100A9* under control of the MHC class I H2K promoter (Cheng et al., 2008) (Figure 6A). S100A8/9 (GFP) was expressed in a mesenchymal (CD45⁻ CD31⁻ Ter119⁻ CD51⁺ Sca1⁻) niche population, previously shown to contain the Osterix-expressing cells (Schepers et al, 2013) (Figure 6B and 6C). The S100A8/9⁺ microenvironment induced

accumulation of superoxide radicals (DHE) and DNA-damage (γ H2AX) in wild type (CD45.1⁺) HSPCs (Figure 6D-6F), in particular in immunophenotypic HSCs, indicating that secretion of S100A8/9 from ancillary cells in the microenvironment is indeed sufficient to induce genotoxic stress in HSCs in a paracrine manner.

Translating these findings to human disease, exposure of human cord blood CD34⁺ HSPCs to human recombinant S100A8/9 at clinically relevant concentrations (Chen et al., 2013 and Supplemental Experimental Procedures) resulted in DNA damage (increased γ H2AX foci), apoptosis and impaired HSPC function (CFU-C) (Figure S7).

Activation of the p53-S100A8/9-TLR axis in mesenchymal niche cells predicts leukemic evolution and clinical outcome in human low-risk MDS

To further define the biologic and clinical significance of these findings, we performed transcriptome sequencing of CD271⁺ niche cells in a prospective, homogeneously treated cohort of low-risk MDS patients ($n = 45$, Figure 7A; Table S6). Expression of *S100A8* and *S100A9* was strongly correlated (Figure 7B, 7C), with a subgroup of MDS patients (17/45; 38%) demonstrating significant overexpression of *S100A8* and *S100A9* (Modified Thompson Tau outlier test) (Figure 7B and 7D), independent of established prognostic factors as defined by the revised International Prognostic Scoring System (IPSS-R) and the MD Anderson risk score (LR-PSS) (Table S6). Transcriptional pathway analysis (GSEA) comparing mesenchymal cells overexpressing S100A8/9 ($n = 17$) to those of niche S100A8/9⁻ patients ($n = 28$) revealed activation of p53 and TLR programs in S100A8/9⁺ mesenchymal cells (Figure 7E), in line with experimental data from the mouse model pointing at the existence of a p53-S100A8/9-TLR axis. Leukemic evolution, defined as the development of frank AML or excess of blasts to WHO RAEB1/ RAEB2 (refractory anemia with excess of blasts), occurred in 5/17 (29.4%) of niche S100A8/9⁺ patients (3 AML, 2 RAEB1/RAEB2) vs. 4/28 (14.2%) in niche S100A8/9⁻ patients (2AML, 2 RAEB1/RAEB2). Time to leukemic evolution was significantly shorter in niche S100A8/9⁺ patients (average 3.4 (1-7.5) vs 18.5 (7-40); $P = 0.03$ by Exact Wilcoxon rank

sum test) resulting in a significantly shorter progression-free survival of niche S100A8/9⁺ patients (median 11.5 vs 53 months, $P = 0.03$) (Figure 7F and 7G). Collectively, the data establish activation of p53-S100A8/9 signaling in mesenchymal niche cells as an independent predictor of disease outcome in human MDS.

DISCUSSION

Genomic stress and the ensuing DNA damage play a pivotal role in the attenuation of normal hematopoiesis in ageing and disease. Mutations accumulate in HSPCs over the lifespan of an organism, but the (patho)physiological sources of genomic stress in HSPCs and their relationship with human bone marrow failure remain incompletely understood. Here, we show that specific inflammatory signals from the mesenchymal niche can induce genotoxic stress in heterotypic stem/progenitor cells and relate this concept to the pathogenesis of two human bone marrow failure and leukemia predisposition syndromes, SDS and MDS.

The data indicate that the mesenchymal niche may actively contribute to the formation of a ‘mutagenic’ environment, adding to our understanding of how a premalignant environment facilitates cancer initiation and evolution. The data argue that this may not only occur through facilitated selection and expansion of genetic clones that stochastically emerge in a permissive environment, but that the mesenchymal niche may be an active participant in driving the genotoxic stress underlying tissue failure and malignant transformation of parenchymal cells.

Notably, leukemic transformation was not observed in mice with targeted deficiency of *Sbds* in mesenchymal cells. Earlier, in a related mouse model of targeted *Dicer1* deletion in MPCs, leukemic transformation was a rare event (Raaijmakers et al., 2010). In the light of our current findings, these observations are likely explained by several factors. First, prolonged exposure to a mutagenic niche, beyond the limited lifespan of OCS mice, may be necessary for the accumulation of genetic damage

required for full transformation. Additionally, the data argue that DNA repair-proficient HSPCs are able to cope with the mutagenic stress induced by their environment through activation of the DDR (as shown by molecular activation of cell cycle checkpoints and apoptosis), preventing the accumulation of stable genetic damage (as demonstrated by comet assays) and maintaining the functional integrity of HSPCs (as shown by repopulation assays).

We propose that in SDS (and possibly other congenital bone marrow failure syndromes) genetically aberrant hematopoietic and niche elements cooperate in driving bone marrow failure and leukemic evolution. Our mouse models of SDS support a view in which hematopoietic cell autonomous loss-of-function of *Sbds* drives neutropenia (Zambetti et al., 2015), while niche alterations in this disease drive myelodysplastic alteration and genotoxic stress. It is conceivable that loss-of-function mutations in *Sbds* in HSPCs further sensitizes HSPCs to the genotoxic effects of the *Sbds*-deficient environment, perhaps through attenuation of DNA damage repair mechanisms. It will thus be of considerable interest to test the hypothesis that a mutagenic environment cooperates with aberrant HSPCs, compromised in their ability to cope with inflammatory genotoxic stress, in leukemia evolution. In this context, the propensity of *Sbds*-deficient cells to accumulate ROS (Ambekar et al., 2010), and their reduced ability to cope with various cellular stressors such as mitotic spindle destabilizing agents, endoplasmic reticulum stress activators, topoisomerase inhibitors and UV irradiation (Austin et al., 2008; Ball et al., 2009) is noteworthy.

The current findings add to emerging insights into the role of innate immune TLR-signaling in the pathogenesis of human MDS. TLR4 and other TLRs are overexpressed in HSPCs from MDS patients (Maratheftis et al., 2007; Wei et al., 2013) and TLR4 expression was shown to correlate with apoptosis in CD34⁺ hematopoietic cells. TLR signaling is constitutively activated in MDS mice with deletion of chromosome 5 (del5q) (Starczynowski et al., 2010) and multiple TLR downstream signaling pathways have been shown to be activated in MDS and related to loss of progenitor cell function (Ganan-Gomez et al., 2015).

Our findings implicate the DAMP S100A8/9 derived from the mesenchymal niche as a driver of TLR signaling in this disease. The unbiased identification of S100A8/9 seems to independently converge with an earlier report implicating S100A8/9 in the pathogenesis of MDS (Chen et al., 2013). In this study it was shown that the plasma concentration of S100A9 was significantly increased in MDS patients (Chen et al., 2013) and S100A8/9 was shown to drive expansion and activation of myeloid-derived suppressor cells (MDSCs) that contributed to cytopenia and myelodysplasia in a murine model of S100A9 overexpression through secretion of suppressive cytokines. It is therefore an intriguing possibility that additional, indirect, biologic effects of S100A8/9 contribute to the hematopoietic phenotype of OCS mice. This may include engagement of other cognate receptors of the protein, including expansion of MDSCs through CD33 signaling (Chen et al., 2013).

In our study S100A8/9 was aberrantly overexpressed in a rare population of mesenchymal niche cells, both in the mouse model and human disease. Typically, expression of the protein is found in myeloid cells, raising the question why S100A8/9 production by (rare) niche cells is more relevant to the biology of HSPC than secretion from myeloid/erythroid cells. While the answer to this question remains speculative in the absence of *in vivo* targeted overexpression studies, it is noteworthy that, in contrast to most cytokines, chemokines and other pro-inflammatory molecules, the local accumulation of S100A8/9 in the environment is very high (up to 100µg/ml and about 50 to 100-fold higher than systemic concentrations), likely caused by attachment to extracellular matrices such as proteoglycans (Vogl et al., 2014). This implicates that the exposure of HSPCs to S100A8/9 is projected to relate strongly to their anatomical proximity to a producing cell. CD271⁺ mesenchymal cells are directly adjacent to CD34⁺ HSPC in human bone marrow (Flores-Figueroa et al., 2012). This notion of ‘spatial relevance’ may also be congruent with recent observations that aberrant overexpression of S100A8/9 in hematopoietic (erythroid) cells within the erythroid island in a model of human 5q⁻ syndrome leads to a predominant erythroid, anemic, phenotype (Schneider et al., 2016).

The mechanisms of S100A8/9 induced DNA damage remain to be fully elucidated. Our experiments using NAC to reduce ROS burden suggest an incomplete association between oxidative stress and DNA damage, suggesting that S100A8/9 secretion may attenuate genomic integrity through additional mechanisms. Similarly, it is conceivable that other ligands secreted from mesenchymal cells contribute to the induction of DNA damage in HSPCs in the mouse model. We found a striking abundance of transcripts encoding other DAMPs and cytotoxic proteins in both the mouse model and mesenchymal elements isolated from SDS patients. Ongoing investigations will have to assess whether other selected ligands can evoke genomic stress in heterotypic HSPCs and in such a fashion contribute to the generation of a mutagenic environment in these disorders.

Finally, our findings establish molecular characteristics of the mesenchymal environment as an important determinant of disease outcome in humans. S100A8/9 expression, associated with activated p53 and TLR signaling, in mesenchymal cells predicted leukemic evolution and progression-free survival in a cohort of homogeneously treated low-risk MDS patients. This is of considerable clinical relevance because low-risk MDS is a heterogeneous disease-entity with a subset of patients having a particular dismal prognosis not identified by current risk-stratification strategies (Bejar et al., 2012). Gene expression of S100A8/9 may identify a substantial subset of patients with a survival typically associated with 'high-risk' patients and, if confirmed in larger independent cohorts, could guide therapeutic decision making in MDS. The data thus provide a strong rationale for niche-instructed therapeutic targeting of inflammatory signaling in human preleukemic disease.

EXPERIMENTAL PROCEDURES

Mice and *in vivo* procedures

OCS, *Trp53^{ff}* and S100A9Tg mice have been previously described (Cheng et al., 2008; Jonkers et al., 2001; Raaijmakers et al., 2010). *Ptprc^aPepc^b/BoyCrl* (B6.SJL) mice were purchased from Charles River. Animals were maintained in specific pathogen free conditions in the Experimental Animal Center of Erasmus MC (EDC). For *in vivo* cell cycle analysis, OCS mice received intraperitoneal injections of BrdU (1.5 mg in PBS, BD Biosciences) and sacrificed after 15 h. For TLR4 studies, 2 week-old mice were intraperitoneally injected with a double dose (100 µg and 35 µg, 48 h interval) of TLR4-neutralizing antibody (clone MTS510, eBioscience) or isotype control (clone eBR2a, eBioscience) and sacrificed after 60h. For NAC rescue studies, 2-week-old mice received daily intraperitoneal injections of NAC (Sigma-Aldrich, 320 mg/kg in saline) until the day of the analysis and at least for 5 days. All mice were sacrificed by cervical dislocation. Animal studies were approved by the Animal Welfare/Ethics Committee of the EDC in accordance with legislation in the Netherlands (Approval No. EMC 2067, 2714, 2892, 3062).

µCT analysis

Femur bones were isolated, fixated in 3% PFA/PBS for 24 h and stored in 70% ethanol. µCT analysis was performed using a SkyScan 1172 system (SkyScan) using previously described settings (Tudpor et al., 2015). Bone microarchitectural parameters relative to the trabecular and the cortical area were determined in the distal metaphysis and the mid-diaphysis of each femur, respectively, using software packages from Bruker MicroCT (NRecon, CtAn and Dataviewer).

Human bone marrow samples

Bone marrow aspirates were obtained from SDS and DBA patients during routine follow-up. All MDS patients were treated with lenalidomide (10 mg/day, d 1-21 in a 4-week schedule) in the context of an ongoing prospective clinical trial for patients with low or intermediate-1 risk MDS according

to IPSS criteria (HOVON89; www.hovon.nl; www.trialregister.nl as NTR1825; EudraCT No. 2008-002195-10). Bone marrow specimens were collected at study entry and disease diagnosis and staging confirmed by central board reviewing. Leukemic evolution was assessed according to WHO criteria; development of RAEB1 (refractory anemia with excess of blast) or RAEB-2 (if RAEB1 at entry) was considered progression of disease. Leukemia (AML) was diagnosed according to standard WHO criteria ($\geq 20\%$ myeloblasts in blood/bone marrow). Bone marrow cells from allogeneic transplantation donors were used as normal controls. Patients and healthy donor characteristics are described in Table S4 and S6. All specimens were collected with informed consent, in accordance with the Declaration of Helsinki

Gene expression profiling

Osx::GFP cells from bone cell suspensions of OCS mice were sorted in TRIzol Reagent (Life Technologies) and RNA was extracted according to the manufacturer's recommendations. Linear amplification of mRNA was performed using the Ovation Pico WTA System (NuGEN). cDNA was fragmented and labelled with Encore™ Biotin Module (NuGEN). The biotinylated cDNA was hybridized to the GeneChip Mouse Genome 430 2.0 Array (Affymetrix eBioscience). Signal was normalized and differential gene expression analysis was performed with the limma package (Ritchie et al., 2015). RNA sequencing experiments were performed as previously described (Zambetti et al., 2015). Human transcripts were aligned to the Ref Seq transcriptome (hg19) and analyzed with DESeq2 (Love et al., 2014), while mouse transcripts were aligned to the Ensembl transcriptome (mm10) and analyzed with EdgeR (Robinson et al., 2010) in the R environment. FPKM values were calculated using Cufflinks (Trapnell et al., 2010). Principal component analysis was performed in the R environment on the raw fragment counts extracted from the BAM files by HTSeq-count (Anders et al., 2015). For Gene Set Enrichment Analysis (Subramanian et al., 2005) (GSEA, Broad Institute), normalized intensity values (microarray data) and FPKM values (RNA sequencing) were compared to the curated gene sets (C2) and the Gene Ontology gene sets (C5) of the Molecular Signature

Database (MsigDB) using the Signal2Noise metric and 1000 gene set-based permutations. For HSPCs GO-term analysis, genes with significantly differential expression ($P < 0.05$) were interrogated using g:Profiler web-based software (Reimand et al., 2011; Reimand et al., 2007).

Immunofluorescence microscopy

HSPCs were harvested in PBS+0.5%FBS, cytopun on a glass slide for 3 min at 500 rpm using a Cytospin 4 centrifuge (Thermo Scientific) and fixed in 3% PFA/PBS for 15 min on ice. After 3 washing steps in PBS, cells were permeabilized for 2 min in 0.15% Triton-X100/PBS. Aspecific binding sites were blocked by incubation in 1%BSA/PBS for 1 h at room temperature. Cells were next stained overnight at 4°C with either anti-phospho-histone H2A.X (Ser139) mouse monoclonal antibody (clone JBW301, Merck Millipore, diluted 1:1000 in 1%BSA/PBS) or with anti-53BP1 rabbit polyclonal antibody (Novus Biologicals, diluted 1:1000 in 1%BSA/PBS). Slides were washed twice in PBS for 5 min and incubated for 1 h at 37°C with either Alexa Fluor 488-conjugated goat anti-mouse antibody (Cat. A10667, Life Technologies) or goat anti-rabbit antibody (Cat. A11008, Life Technologies), both diluted 1:200 in 1%BSA/PBS. After 2 washes in PBS, slides were mounted in VECTASHIELD Mounting Medium with DAPI (Vector Laboratories). Z-series images were acquired with a Leica TCS SP5 confocal microscope (63X objective lens) using the LAS software (Leica Microsystems). γ H2AX and 53BP1 foci were counted manually from the maximum projection view.

Survival analysis

The low-risk MDS patient subgroup with S100 niche signature was defined by the Modified Thompson Tau test for outlier detection. In brief, *S100A8* statistics from the control cases were combined to define the rejection region, demarcating FPKM values to be considered as outliers. MDS cases with *S100A8* FPKM values within the rejection region were thus defined as niche-signature⁺. To determine the significance difference in time to progression we used the Wilcoxon signed rank

test accounting for tied observations. Event-free survival was determined by specifying leukemic progression or death as events. Patients experiencing a non-hematological related death (e.g., cardiac failure), were censored on the date of this event. Patients remaining alive were censored on the date of last consultation. Kaplan-Meier curves were used to estimate the survival functions through time. Statistical differences in the survival distributions was assessed with the Mantel-Cox log-rank test. All calculations were performed in the R environment.

Statistics

Statistical analysis was performed using Prism 5 (GraphPad Software). Unless otherwise specified, unpaired, 2-tailed Student's t test (single test) or 1-way analysis of variance (multiple comparisons) were used to evaluate statistical significance, defined as $P < 0.05$. All results in bar graphs are mean value \pm standard error of the mean.

SUPPLEMENTAL INFORMATION

Supplemental Information includes Supplemental Experimental Procedures, five figures, and six tables.

AUTHOR CONTRIBUTIONS

Conceptualization: N.A.Z. and M.H.G.P.R.; Methodology: N.A.Z., Z.P., S.C., K.J.G.K., E.M.J.B., B.V.D.E., M.A.M., J.P.T.M.V.L., R.K., T.V., and M.H.G.P.R.; Investigation: N.A.Z., Z.P., S.C., E.M.J.B., B.V.D.E., M.N.A., P.M.H.V.S., C.V.D.L., M.K., M.A.M., and T.V.; Resources: T.W.K., T.M.W., A.V.D.L., E.M.K., C. M., P. G. M., J.P.T.M.V.L, R.K., I.P.T. and T.V.; Data curation: M.A.S., R.M.H., T.W.K., T.M.W., A.V.D.L., and E.M.K.; Writing: N.A.Z. and M.H.G.P.R; Visualization: N.A.Z., Z.P., S.C, and R.H.M. ; Supervision and Funding Acquisition: M.H.G.P.R.

ACKNOWLEDGEMENTS

Prof. Johanna M. Rommens donated *Sbds*-floxed mice; Dr Eric Braakman and Mariette ter Borg provided CD34⁺ cells; Dr Elwin Rombouts, Onno Roovers, Peter van Geel, Marijke Koedam, Nicole van Vliet, Charlie Laffeber and Gert-Jan Kremers provided technical assistance; Dr Marc Bierings and Dr Valerie de Haas on behalf of the ‘Stichting Kinderoncologie Nederland (SKION)’ provided DBA samples; Pearl F.M. Mau Asam helped with SDS bone marrow collection; Dr Dana Chitu of the HOVON data center helped with clinical data; members of the Erasmus MC Department of Hematology provided scientific discussion; members of the Erasmus MC animal core facility EDC helped with animal care. This work was supported by grants from the Dutch Cancer Society (KWF Kankerbestrijding), Amsterdam, The Netherlands (grant EMCR 2010-4733 to M.H.G.P.R.), the Netherlands Organization of Scientific Research (NWO 90700422 to M.H.G.P.R.) and the Netherlands Genomics Initiative (Zenith grant no 40-41009-98-11062 to M.H.G.P.R.).

REFERENCES

- Aggett, P.J., Cavanagh, N.P.C., Matthew, D.J., Pincott, J.R., Sutcliffe, J., and Harries, J.T. (1980). Shwachmans Syndrome - a Review of 21 Cases. *Arch. Dis. Child.* 55, 331-347.
- Alter, B.P. (2007). Diagnosis, genetics, and management of inherited bone marrow failure syndromes. *Hematology Am. Soc. Hematol. Educ. Program*, 29-39.
- Ambekar, C., Das, B., Yeager, H., and Dror, Y. (2010). SBDS-deficiency results in deregulation of reactive oxygen species leading to increased cell death and decreased cell growth. *Pediatr. Blood Cancer* 55, 1138-1144.
- Anders, S., Pyl, P.T., and Huber, W. (2015). HTSeq--a Python framework to work with high-throughput sequencing data. *Bioinformatics* 31, 166-169.
- Arranz, L., Sanchez-Aguilera, A., Martin-Perez, D., Isern, J., Langa, X., Tzankov, A., Lundberg, P., Muntion, S., Tzeng, Y.S., Lai, D.M., *et al.* (2014). Neuropathy of haematopoietic stem cell niche is essential for myeloproliferative neoplasms. *Nature* 512, 78-81.
- Austin, K.M., Gupta, M.L., Jr., Coats, S.A., Tulpule, A., Mostoslavsky, G., Balazs, A.B., Mulligan, R.C., Daley, G., Pellman, D., and Shimamura, A. (2008). Mitotic spindle destabilization and genomic instability in Shwachman-Diamond syndrome. *J. Clin. Invest.* 118, 1511-1518.
- Ball, H.L., Zhang, B., Riches, J.J., Gandhi, R., Li, J., Rommens, J.M., and Myers, J.S. (2009). Shwachman-Bodian Diamond syndrome is a multi-functional protein implicated in cellular stress responses. *Hum. Mol. Genet.* 18, 3684-3695.
- Bejar, R., Stevenson, K.E., Caughey, B.A., Abdel-Wahab, O., Steensma, D.P., Galili, N., Raza, A., Kantarjian, H., Levine, R.L., Neuberg, D., *et al.* (2012). Validation of a prognostic model and the impact of mutations in patients with lower-risk myelodysplastic syndromes. *J. Clin. Oncol.* 30, 3376-3382.

Boocock, G.R., Morrison, J.A., Popovic, M., Richards, N., Ellis, L., Durie, P.R., and Rommens, J.M. (2003). Mutations in SBDS are associated with Shwachman-Diamond syndrome. *Nat. Genet.* *33*, 97-101.

Chen, S., Zambetti, N.A., Bindels, E.M., Kenswill, K., Mylona A.M., Adisty, N.M., Hoogenboezem, R.M., Sanders, M.A., Cremers, E.M., Westers, T.M., *et al.* (2016). Massive parallel RNA sequencing of highly purified mesenchymal elements in low-risk MDS reveals tissue-context-dependent activation of inflammatory programs. *Leukemia* <http://dx.doi.org/10.1038/leu.2016.91>.

Chen, X., Eksioglu, E.A., Zhou, J., Zhang, L., Djeu, J., Fortenbery, N., Epling-Burnette, P., Van Bijnen, S., Dolstra, H., Cannon, J., *et al.* (2013). Induction of myelodysplasia by myeloid-derived suppressor cells. *J. Clin. Invest.* *123*, 4595-4611.

Cheng, P., Corzo, C.A., Luetkeke, N., Yu, B., Nagaraj, S., Bui, M.M., Ortiz, M., Nacken, W., Sorg, C., Vogl, T., *et al.* (2008). Inhibition of dendritic cell differentiation and accumulation of myeloid-derived suppressor cells in cancer is regulated by S100A9 protein. *J. Exp. Med.* *205*, 2235-2249.

Curtin, N.J. (2012). DNA repair dysregulation from cancer driver to therapeutic target. *Nat. Rev. Cancer* *12*, 801-817.

Donadieu, J., Fenneteau, O., Beaupain, B., Beaufils, S., Bellanger, F., Mahlaoui, N., Lambilliotte, A., Aladjidi, N., Bertrand, Y., Mialou, V., *et al.* (2012). Classification of and risk factors for hematologic complications in a French national cohort of 102 patients with Shwachman-Diamond syndrome. *Haematologica* *97*, 1312-1319.

Finch, A.J., Hilcenko, C., Basse, N., Drynan, L.F., Goyenechea, B., Menne, T.F., Fernandez, A.G., Simpson, P., D'Santos, C.S., Arends, M.J., *et al.* (2011). Uncoupling of GTP hydrolysis from eIF6 release on the ribosome causes Shwachman-Diamond syndrome. *Genes Dev.* *25*, 917-929.

Flores-Figueroa, E., Varma, S., Montgomery, K., Greenberg, P.L., Gratzinger, D. (2012). Distinctive contact between CD34+ hematopoietic progenitors and CXCL12+ CD271+ mesenchymal stromal cells in benign and myelodysplastic bone marrow. *Lab. Invest.* *92*, 1330-1341.

Ganan-Gomez, I., Wei, Y., Starczynowski, D.T., Colla, S., Yang, H., Cabrero-Calvo, M., Bohannon, Z.S., Verma, A., Steidl, U., and Garcia-Manero, G. (2015). Deregulation of innate immune and inflammatory signaling in myelodysplastic syndromes. *Leukemia* 29, 1458-1469.

Ginzberg, H., Shin, J., Ellis, L., Morrison, J., Ip, W., Dror, Y., Freedman, M., Heitlinger, L.A., Belt, M.A., Corey, M., *et al.* (1999). Shwachman syndrome: phenotypic manifestations of sibling sets and isolated cases in a large patient cohort are similar. *J. Pediatr.* 135, 81-88.

Hanoun, M., Zhang, D., Mizoguchi, T., Pinho, S., Pierce, H., Kunisaki, Y., Lacombe, J., Armstrong, S.A., Duhrsen, U., and Frenette, P.S. (2014). Acute myelogenous leukemia-induced sympathetic neuropathy promotes malignancy in an altered hematopoietic stem cell niche. *Cell Stem Cell* 15, 365-375.

Head, D.R., Jacobberger, J.W., Mosse, C., Jagasia, M., Dupont, W., Goodman, S., Flye, L., Shinar, A., McClintock-Treep, S., Stelzer, G., *et al.* (2011). Innovative analyses support a role for DNA damage and an aberrant cell cycle in myelodysplastic syndrome pathogenesis. *Bone Marrow Res.* 2011, 950934.

Ito, K., Hirao, A., Arai, F., Takubo, K., Matsuoka, S., Miyamoto, K., Ohmura, M., Naka, K., Hosokawa, K., Ikeda, Y., *et al.* (2006). Reactive oxygen species act through p38 MAPK to limit the lifespan of hematopoietic stem cells. *Nat. Med.* 12, 446-451.

Jaiswal, S., Fontanillas, P., Flannick, J., Manning, A., Grauman, P.V., Mar, B.G., Lindsley, R.C., Mermel, C.H., Burt, N., Chavez, A., *et al.* (2014). Age-related clonal hematopoiesis associated with adverse outcomes. *N. Engl. J. Med.* 371, 2488-2498.

Jonkers, J., Meuwissen, R., van der Gulden, H., Peterse, H., van der Valk, M., and Berns, A. (2001). Synergistic tumor suppressor activity of BRCA2 and p53 in a conditional mouse model for breast cancer. *Nat. Genet.* 29, 418-425.

Kode, A., Manavalan, J.S., Mosialou, I., Bhagat, G., Rathinam, C.V., Luo, N., Khiabani, H., Lee, A., Murty, V.V., Friedman, R., *et al.* (2014). Leukaemogenesis induced by an activating beta-catenin mutation in osteoblasts. *Nature* 506, 240-244.

Li, C., Chen, H., Ding, F., Zhang, Y., Luo, A., Wang, M., and Liu, Z. (2009). A novel p53 target gene, S100A9, induces p53-dependent cellular apoptosis and mediates the p53 apoptosis pathway. *Biochem. J.* *422*, 363-372.

Li, L., Li, M., Sun, C., Francisco, L., Chakraborty, S., Sabado, M., McDonald, T., Gyorffy, J., Chang, K., Wang, S., *et al.* (2011). Altered hematopoietic cell gene expression precedes development of therapy-related myelodysplasia/acute myeloid leukemia and identifies patients at risk. *Cancer Cell* *20*, 591-605.

Love, M.I., Huber, W., and Anders, S. (2014). Moderated estimation of fold change and dispersion for RNA-seq data with DESeq2. *Genome Biol.* *15*, 550.

Mäkitie, O., Ellis, L., Durie, P.R., Morrison, J.A., Sochett, E.B., Rommens, J.M., and Cole, W.G. (2004). Skeletal phenotype in patients with Shwachman-Diamond syndrome and mutations in SBDS. *Clin. Genet.* *65*, 101-112.

Maratheftis, C.I., Andreakos, E., Moutsopoulos, H.M., and Voulgarelis, M. (2007). Toll-like receptor-4 is up-regulated in hematopoietic progenitor cells and contributes to increased apoptosis in myelodysplastic syndromes. *Clin. Cancer Res.* *13*, 1154-1160.

Marino, S., Vooijs, M., van der Gulden, H., Jonkers, J., and Berns, A. (2000). Induction of medulloblastomas in p53-null mutant mice by somatic inactivation of Rb in the external granular layer cells of the cerebellum. *Genes Dev.* *14*, 994-1004.

Medyouf, H., Mossner, M., Jann, J.C., Nolte, F., Raffel, S., Herrmann, C., Lier, A., Eisen, C., Nowak, V., Zens, B., *et al.* (2014). Myelodysplastic cells in patients reprogram mesenchymal stromal cells to establish a transplantable stem cell niche disease unit. *Cell Stem Cell* *14*, 824-837.

Murphy, M.P. (2009). How mitochondria produce reactive oxygen species. *Biochem. J.* *417*, 1-13.

Owusu-Ansah, E., Yavari, A., Mandal, S., and Banerjee, U. (2008). Distinct mitochondrial retrograde signals control the G1-S cell cycle checkpoint. *Nat Genet.* *40*, 356-361.

Peddie, C.M., Wolf, C.R., McLellan, L.I., Collins, A.R., and Bowen, D.T. (1997). Oxidative DNA damage in CD34+ myelodysplastic cells is associated with intracellular redox changes and elevated plasma tumour necrosis factor-alpha concentration. *Br. J. Haematol.* *99*, 625-631.

Raaijmakers, M.H., Mukherjee, S., Guo, S., Zhang, S., Kobayashi, T., Schoonmaker, J.A., Ebert, B.L., Al-Shahrour, F., Hasserjian, R.P., Scadden, E.O., *et al.* (2010). Bone progenitor dysfunction induces myelodysplasia and secondary leukaemia. *Nature* *464*, 852-857.

Raiser, D.M., Narla, A., and Ebert, B.L. (2014). The emerging importance of ribosomal dysfunction in the pathogenesis of hematologic disorders. *Leuk. Lymphoma* *55*, 491-500.

Rawls, A.S., Gregory, A.D., Woloszynek, J.R., Liu, F.L., and Link, D.C. (2007). Lentiviral-mediated RNAi inhibition of Sbds in murine hematopoietic progenitors impairs their hematopoietic potential. *Blood* *110*, 2414-2422.

Reimand, J., Arak, T., and Vilo, J. (2011). g:Profiler--a web server for functional interpretation of gene lists (2011 update). *Nucleic Acids Res.* *39*, W307-315.

Reimand, J., Kull, M., Peterson, H., Hansen, J., and Vilo, J. (2007). g:Profiler--a web-based toolset for functional profiling of gene lists from large-scale experiments. *Nucleic Acids Res.* *35*, W193-200.

Ritchie, M.E., Phipson, B., Wu, D., Hu, Y., Law, C.W., Shi, W., and Smyth, G.K. (2015). limma powers differential expression analyses for RNA-sequencing and microarray studies. *Nucleic Acids Res.* *43*, e47.

Robinson, M.D., McCarthy, D.J., and Smyth, G.K. (2010). edgeR: a Bioconductor package for differential expression analysis of digital gene expression data. *Bioinformatics* *26*, 139-140.

Rossi, D.J., Bryder, D., Seita, J., Nussenzweig, A., Hoeijmakers, J., and Weissman, I.L. (2007). Deficiencies in DNA damage repair limit the function of haematopoietic stem cells with age. *Nature* *447*, 725-729.

Sahin, E., and Depinho, R.A. (2010). Linking functional decline of telomeres, mitochondria and stem cells during ageing. *Nature* *464*, 520-528.

Schepers, K., Campbell, T.B., and Passegue, E. (2015). Normal and leukemic stem cell niches: insights and therapeutic opportunities. *Cell Stem Cell* *16*, 254-267.

Schepers, K., Pietras, E.M., Reynaud, D., Flach, J., Binnewies, M., Garg, T., Wagers, A.J., Hsiao, E.C., and Passegué, E. (2013). Myeloproliferative neoplasia remodels the endosteal bone marrow niche into a self-reinforcing leukemic niche. *Cell Stem Cell* *13*, 285-299.

Schneider, R.K., Schenone, M., Ferreira, M.V., Kramann, R., Joyce, C.E., Hartigan, C., Beier, F., Brümmendorf, T.H., Germing, U., Platzbecker, U. *et al.* (2016). Rps14 haploinsufficiency causes a block in erythroid differentiation mediated by S100A8 and S100A9. *Nat. Med.* *22*, 288-297.

Srikrishna, G., and Freeze, H.H. (2009). Endogenous damage-associated molecular pattern molecules at the crossroads of inflammation and cancer. *Neoplasia* *11*, 615-628.

Stowe, D.F., and Camara, A.K.S. (2009). Mitochondrial Reactive Oxygen Species Production in Excitable Cells: Modulators of Mitochondrial and Cell Function. *Antioxid. Redox Signal.* *11*, 1373-1414.

Subramanian, A., Tamayo, P., Mootha, V.K., Mukherjee, S., Ebert, B.L., Gillette, M.A., Paulovich, A., Pomeroy, S.L., Golub, T.R., Lander, E.S., *et al.* (2005). Gene set enrichment analysis: a knowledge-based approach for interpreting genome-wide expression profiles. *Proc. Natl. Acad. Sci. USA* *102*, 15545-15550.

Toiviainen-Salo, S., Mayranpaa, M.K., Durie, P.R., Richards, N., Grynopas, M., Ellis, L., Ikegawa, S., Cole, W.G., Rommens, J., Marttinen, E., *et al.* (2007). Shwachman-Diamond syndrome is associated with low-turnover osteoporosis. *Bone* *41*, 965-972.

Tormin, A., Li, O., Brune, J.C., Walsh, S., Schutz, B., Ehinger, M., Ditzel, N., Kassem, M., and Scheduling, S. (2011). CD146 expression on primary nonhematopoietic bone marrow stem cells is correlated with in situ localization. *Blood* *117*, 5067-5077.

Starczynowski, D.T., Kuchenbauer, F., Argiropoulos, B., Sung, S., Morin, R., Muranyi, A., Hirst, M., Hogge, D., Marra, M., Wells, R.A., *et al.* (2010). Identification of miR-145 and miR-146a as mediators of the 5q- syndrome phenotype. *Nat. Med.* *16*, 49-58.

Trapnell, C., Williams, B.A., Pertea, G., Mortazavi, A., Kwan, G., van Baren, M.J., Salzberg, S.L., Wold, B.J., and Pachter, L. (2010). Transcript assembly and quantification by RNA-Seq reveals unannotated transcripts and isoform switching during cell differentiation. *Nat. Biotechnol.* 28, 511-515.

Tudpor, K., van der Eerden, B.C., Jongwattanasrisan, P., Roelofs, J.J., van Leeuwen, J.P., Bindels, R.J., and Hoenderop, J.G. (2015). Thrombin receptor deficiency leads to a high bone mass phenotype by decreasing the RANKL/OPG ratio. *Bone* 72, 14-22.

Vlachos, A., Rosenberg, P.S., Atsidaftos, E., Alter, B.P., and Lipton, J.M. (2012). Incidence of neoplasia in Diamond Blackfan anemia: a report from the Diamond Blackfan Anemia Registry. *Blood* 119, 3815-3819.

Vogl, T., Eisenblätter, M., Völler, T., Zenker, S., Hermann, S., van Lent, P., Faust, A., Geyer, C., Petersen, B., Roebrock, K., *et al.* (2014). Alarmin S100A8/S100A9 as a biomarker for molecular imaging of local inflammatory activity. *Nat. Commun.* 6,4593.

Vogl, T., Tenbrock, K., Ludwig, S., Leukert, N., Ehrhardt, C., van Zoelen, M.A., Nacken, W., Foell, D., van der Poll, T., Sorg, C., *et al.* (2007). Mrp8 and Mrp14 are endogenous activators of Toll-like receptor 4, promoting lethal, endotoxin-induced shock. *Nat. Med.* 13, 1042-1049.

Walkley, C.R., Olsen, G.H., Dworkin, S., Fabb, S.A., Swann, J., McArthur, G.A., Westmoreland, S.V., Chambon, P., Scadden, D.T., and Purton, L.E. (2007). A microenvironment-induced myeloproliferative syndrome caused by retinoic acid receptor gamma deficiency. *Cell* 129, 1097-1110.

Walter, D., Lier, A., Geiselhart, A., Thalheimer, F.B., Huntscha, S., Sobotta, M.C., Moehrle, B., Brocks, D., Bayindir, I., Kaschutnig, P., *et al.* (2015). Exit from dormancy provokes DNA-damage-induced attrition in haematopoietic stem cells. *Nature* 520, 549-552.

Wang, X., Kua, H.Y., Hu, Y., Guo, K., Zeng, Q., Wu, Q., Ng, H.H., Karsenty, G., de Crombrughe, D., Yeh, J., *et al.* (2006). p53 functions as a negative regulator of osteoblastogenesis, osteoblast-dependent osteoclastogenesis, and bone remodeling. *J. Cell. Biol.* 172, 115-125.

Wei, Y., Dimicoli, S., Bueso-Ramos, C., Chen, R., Yang, H., Neuberg, D., Pierce, S., Jia, Y., Zheng, H., Wang, H., *et al.* (2013). Toll-like receptor alterations in myelodysplastic syndrome. *Leukemia* 27, 1832-1840.

Woloszynek, J.R., Rothbaum, R.J., Rawls, A.S., Minx, P.J., Wilson, R.K., Mason, P.J., Bessler, M., and Link, D.C. (2004). Mutations of the SBDS gene are present in most patients with Shwachman-Diamond syndrome. *Blood* 104, 3588-3590.

Xiao, Y., Wang, J., Song, H., Zou, P., Zhou, D., and Liu, L. (2013). CD34+ cells from patients with myelodysplastic syndrome present different p21 dependent premature senescence. *Leuk. Res.* 37, 333-340.

Yahata, T., Takanashi, T., Muguruma, Y., Ibrahim, A.A., Matsuzawa, H., Uno, T., Sheng, Y., Onizuka, M., Ito, M., Kato, S., *et al.* (2011). Accumulation of oxidative DNA damage restricts the self-renewal capacity of human hematopoietic stem cells. *Blood* 118, 2941-2950.

Zambetti, N.A., Bindels, E.M., Van Strien, P.M., Valkhof, M.G., Adisty, M.N., Hoogenboezem, R.M., Sanders, M.A., Rommens, J.M., Touw, I.P., and Raaijmakers, M.H. (2015). Deficiency of the ribosome biogenesis gene *Sbds* in hematopoietic stem and progenitor cells causes neutropenia in mice by attenuating lineage progression in myelocytes. *Haematologica*.

FIGURE LEGENDS

Figure 1. Deletion of *Sbds* in MPCs recapitulates skeletal defects in human SDS. (A-B) Impaired growth in OCS^{f/f} mice: (A) body weight ($n = 9$) and (B) femur length ($n = 5$). (C-H) Femur μ CT analysis of OCS^{f/+} ($n = 5$) and OCS^{f/f} ($n = 4$) mice. (C) Representative 2D-images. Left: longitudinal view. Right: cortical bone. (D) 3D-image. (E) Bone volume per tissue volume (BV/TV). (F) Trabecular number (Tb. N). (G) Trabecular spacing (Tb. Sp). (H) Cortical bone mineral density (BMD). (I) Goldner osteoblast staining (OCS^{f/+}, $n = 6$; OCS^{f/f}, $n = 8$). Left: representative images (arrows: osteoblasts; with white dashed line in the magnified region). Right: number of osteoblasts per bone perimeter (N.Ob/B.Pm). (J-K) 3-point bending test indicating (J) reduced resistant to fracture and (K) decreased stiffness of OCS^{f/f} bone (OCS^{f/+}, $n = 5$; OCS^{f/f}, $n = 4$). * $P < 0.05$. ** $P < 0.01$. *** $P < 0.001$. Data are mean \pm SEM. See also Figure S1.

Figure 2. *Sbds*-deficient mesenchymal cells induce genotoxic stress in HSPCs. (A) Transcriptional network analysis indicating mitochondrial dysregulation in mutant HSPCs. NES: Normalized Enrichment Score. (B-C) Increased mitochondrial potential (TMRM) in HSPCs: (B) representative plots; (C) mean fluorescence intensity (MFI) ($n = 3$). (D) ROS quantification by CM-H2DCFDA (OCS^{f/+}, $n = 6$; OCS^{f/f}, $n = 7$). (E) Increased γ H2AX levels in mutant HSPCs. Left, representative FACS analysis. Right, MFI values ($n = 4$). (F-I) Activation of DNA damage response in mutant HSPCs. (F) Transcriptional repression of G1-S checkpoint progression. (G, H) *In vivo* BrdU staining confirming impaired S-phase transition ($n = 4$). (I) Downregulation of Myc signaling. GSEA data shown is from CD48⁻ LKS cells. a.u., arbitrary units. †††FDR<0.001. * $P < 0.05$. ** $P < 0.01$. *** $P < 0.001$. Data in bar graphs are mean \pm SEM. See also Figure S2, S3, S6 and Table S1-S3.

Figure 3. Activation of p53 in MPCs drives skeletal and hematopoietic abnormalities in OCS mutants. (A) p53 protein (FACS) accumulates in GFP⁺ cells from OCS^{f/f} mice ($n = 3$). (B-C) Activation of p53 in mutant GFP⁺ cells as demonstrated by (B) enrichment of a p53 GSEA signature and (C) overexpression of canonical p53 targets ($n = 3$). (D) Schematic representation of the p53

floxed allele with indication of primers used to assess genotypes (p10.1-p10.2) and genomic deletion (p1.1-p10.2). (E) Specific deletion of p53 in bone-containing tissue in OCS^{f/f} p53^Δ mice (genomic PCR). (F-J) μCT analysis indicating normalization of bone mass in OCS^{f/f} mice upon genetic deletion of p53 (p53⁺, *n* = 3; p53^Δ, *n* = 5). Tb. Pf, Trabecular bone pattern factor. (K) Bone mineral density in OCS^{f/f} mice is not rescued by p53 deletion. (L-M) Effects of p53 deficiency on OCS HSPCs. Tendency for reduced oxidative stress as assessed by DHE analysis (L) and significant reduction of γH2AX levels (M) in HSPCs from OCS^{f/f} p53^Δ mice (*n* = 3). MFI: mean fluorescence intensity. a.u., arbitrary units. **P* < 0.05. ***P* < 0.01. ****P* < 0.001. Data are mean ± SEM. See also Figure S4.

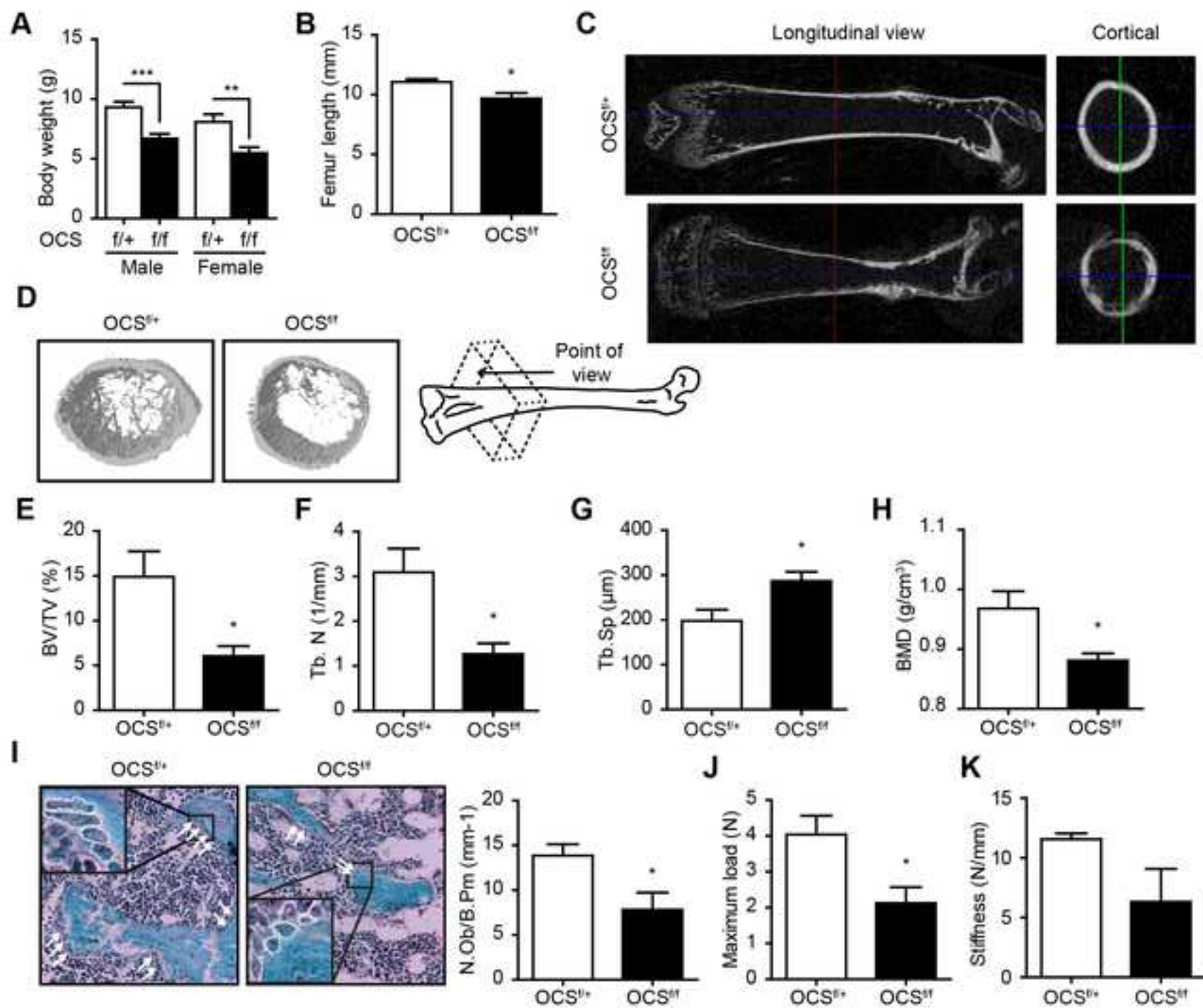
Figure 4. Identification of *S100A8* and *S100A9* as candidate drivers of genotoxic stress in leukemia predisposition syndromes. (A) Representative mesenchymal CD271⁺ FACS gating. (B) Pathognomonic 183-184 TA>CT mutation in niche cells from a representative SDS patient (IGV plot). (C) Reduced *SBDS* expression in SDS niche cells. (D) Disruption of ribosome biogenesis and translation in SDS CD271⁺ cells (GSEA). (E) Inflammation-related transcripts are upregulated in niche cells from SDS patients and OCS^{f/f} mice. (F) Significantly differentially expressed genes in SDS (*n* = 4), MDS (*n* = 9) and DBA (*n* = 3) in comparison to normal CD271⁺ cells. (G) Expression of *S100A8* and *S100A9* in mesenchymal cells from SDS, low-risk MDS, and DBA patients. **P* < 0.05. ****P* < 0.001. †††FDR-adjusted *P* < 0.001. See also Figure S1, S5 and Table S4.

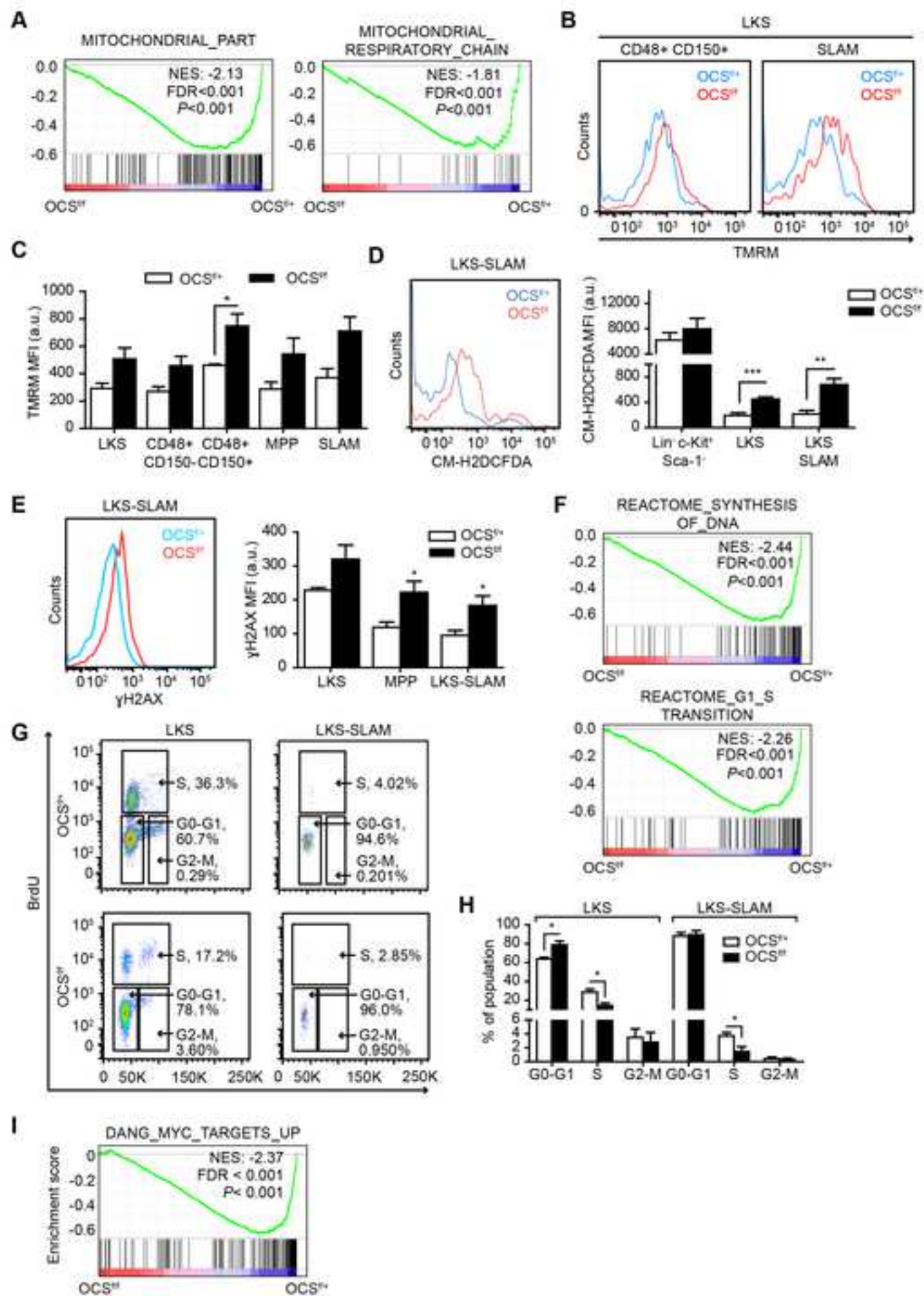
Figure 5. *S100A8/9* induces genotoxic stress in murine HSPCs through TLR4 signaling. (A-B) Increased *S100A8* and *S100A9* levels in OCS^{f/f} GFP⁺ cells. (A) representative plots. (B) MFI values (*n* = 5). (C) Increased plasma concentration of *S100A8/9* by ELISA (OCS^{f/+}, *n* = 5; OCS^{f/f}, *n* = 4). (D) Left: representative γH2AX pictures after HSPCs in vitro exposure. Positive control: 8-Gy irradiated Lin⁻ c-Kit⁺ Sca-1⁻ cells. Negative controls: heat-inactivated *S100A8/9* (H.I. ctr). Right: number of γH2AX foci (*n* = 3). (E) *S100A8/9* has no effect on cell cycle (*n* = 2). (F) Increased apoptosis in *S100A8/9*-exposed LKS (*n* = 3). (G) Activation of TLR signaling (GSEA). (H) TLR4-

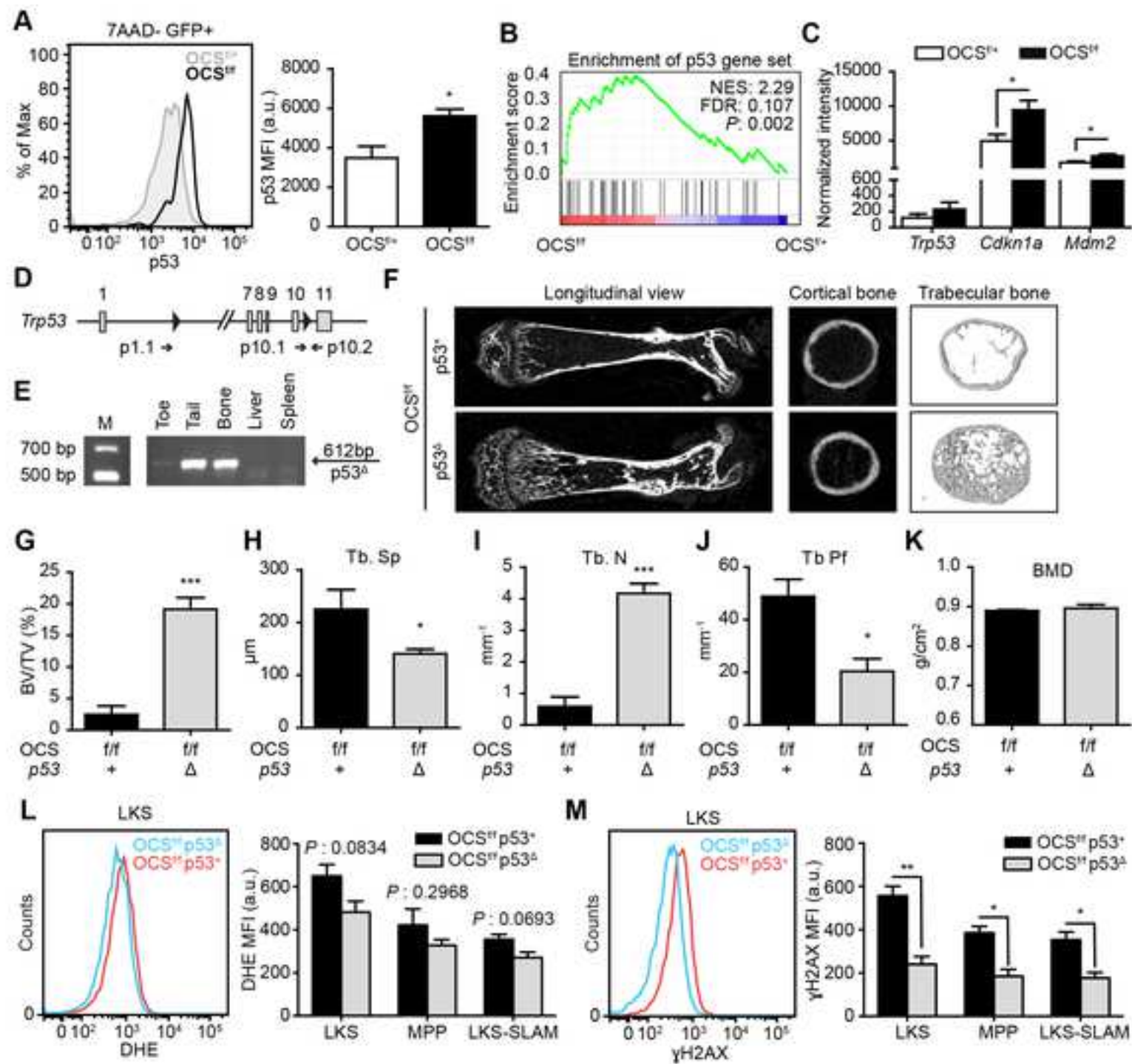
blocking antibodies limit DNA damage in OCS^{ff} mice ($n = 4$). * $P < 0.05$. ** $P < 0.01$. *** $P < 0.001$. Data are mean \pm SEM. See also Figure S6 and S7; Table S5.

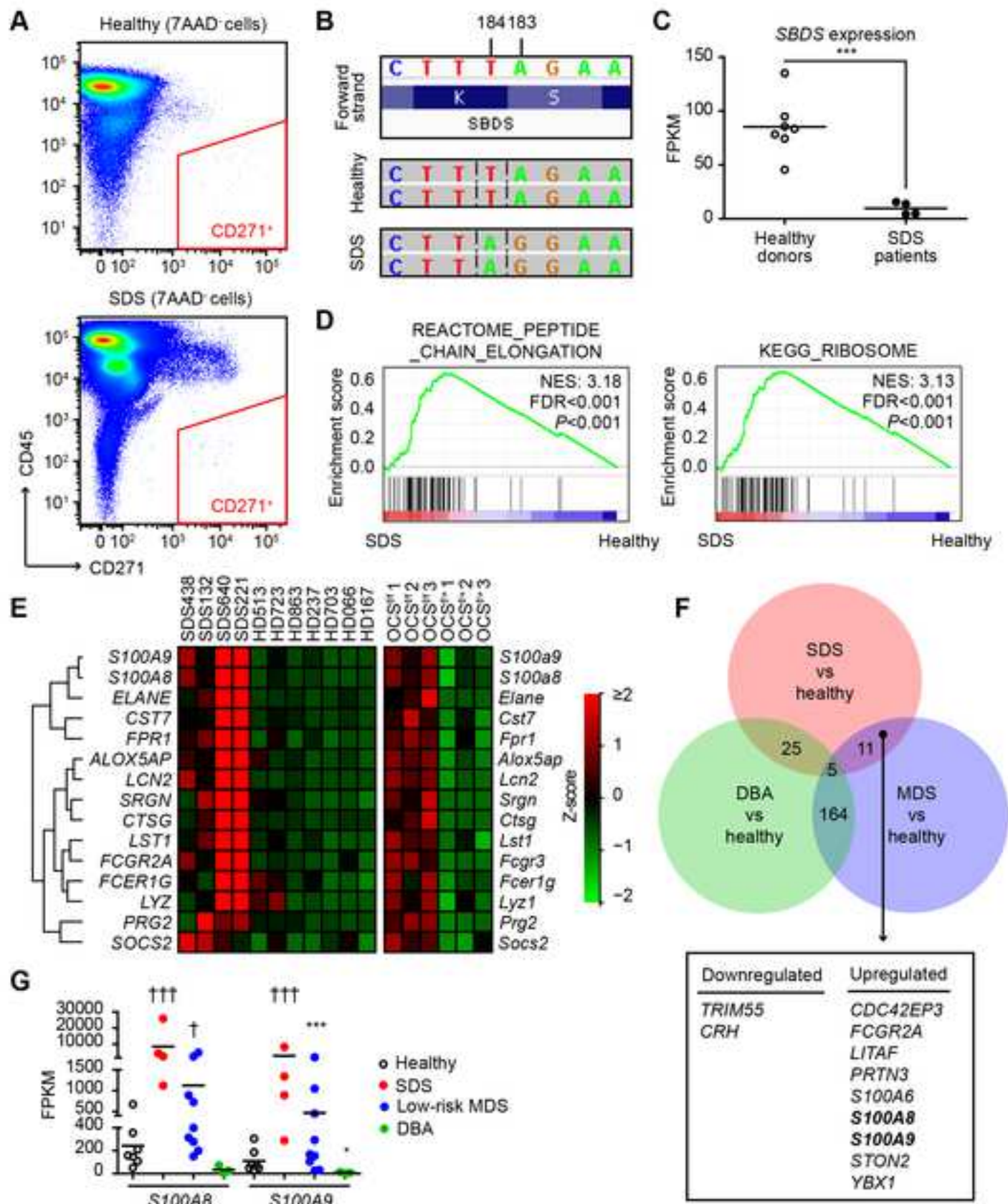
Figure 6. Niche derived S100A8/9 induces oxidative and genotoxic stress in HSPCs. (A) Schematic representation of wild type HSPCs transplantation in S100A9Tg mice. BM: bone marrow. (B-C) Mesenchymal cells from S100A9Tg mice express the S100A9-IRES-GFP construct. (B) Gating strategy defining CD51⁺ Sca-1⁺ mesenchymal ‘stem’ cells (MSC) and CD51⁺ Sca-1⁻ osteolineage cells in the microenvironment (C) Expression of GFP in S100A9Tg-derived mesenchymal compartments ($n = 3$). (D) Transplantation efficiency as assessed by CD45.1⁺ cell chimerism in the bone marrow (BM) of transplanted mice ($n = 4$). (E) Accumulation of superoxide radicals in HSPCs exposed to S100A8/9-overexpressing microenvironment. Left, representative plot. Right, DHE MFI values ($n = 4$). (F) Increased levels of γ H2AX in immunophenotypically-defined HSCs. Left, representative plot. Right, DHE MFI values ($n = 4$). * $P < 0.05$. ** $P < 0.01$. Data are mean \pm SEM.

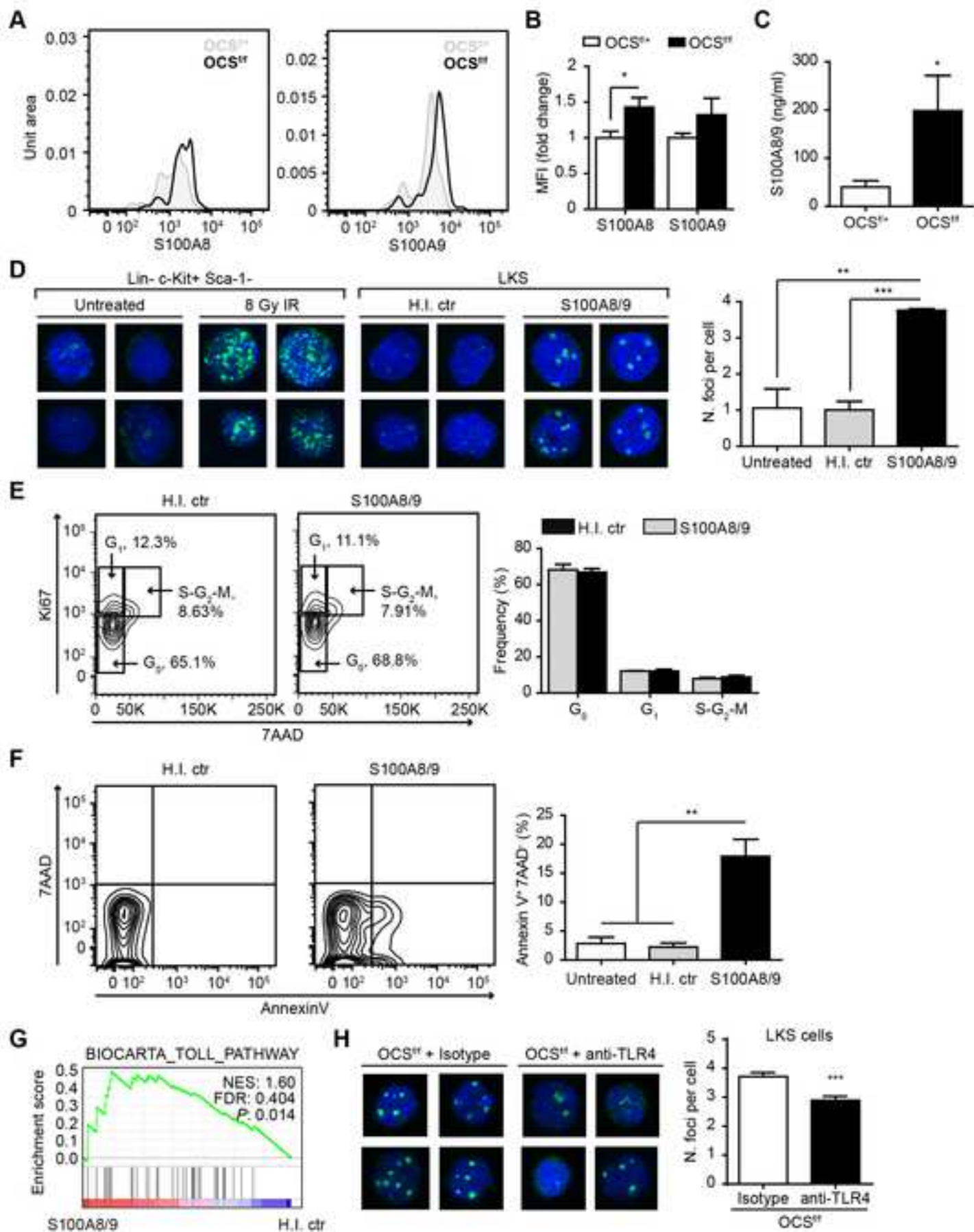
Figure 7. Activation of the p53-S100A8/9-TLR axis in mesenchymal niche cells predicts leukemic evolution and clinical outcome in human low-risk MDS. (A) Representative examples of FACS-isolated CD271⁺ niche cells in human MDS. (B) Correlation plot of *S100A8* and *S100A9* expression levels in human low-risk MDS ($n = 45$). (C) Expression of the defining gene *NGFR* (CD271) in mesenchymal cells (S100 niche +, $n = 17$; S100 niche -, $n = 28$). (D) Representative staining of S100A8 and S100A9 in endosteal (CD271⁺) stromal cells. Intramedullary staining reflects expression of S100A8/9 in myeloid cells. (E) GSEA analysis indicating enrichment of p53 and TLR signatures in S100A8/9-overexpressing CD271⁺ cells. Two representative GSEA plots are shown. NES: Normalized Enrichment Score. (F) Kaplan-Meier survival curve showing progression-free survival (G). Statistical analysis indicating significantly reduced time to progression and progression-free survival (PFS). See also Table S6.

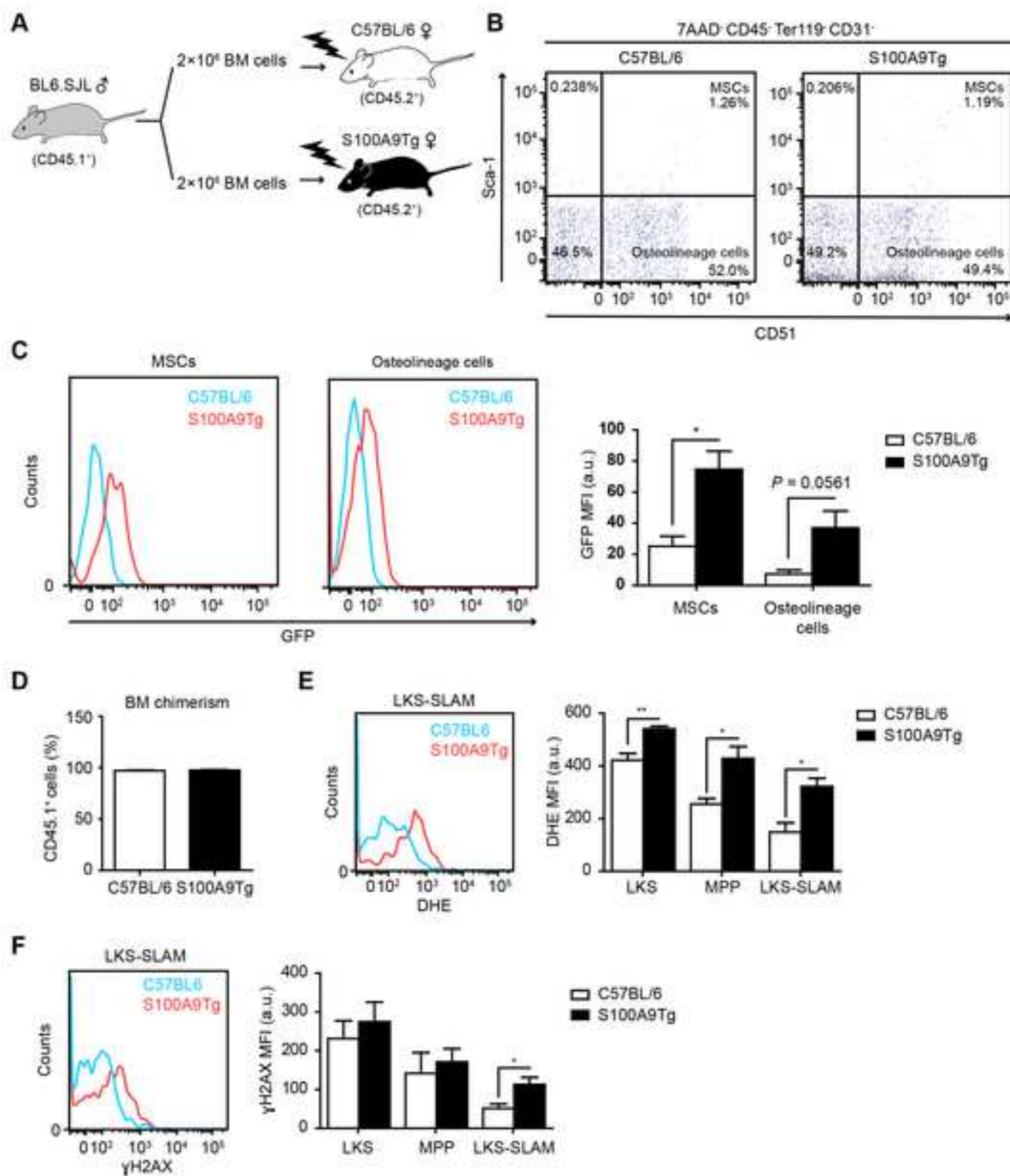


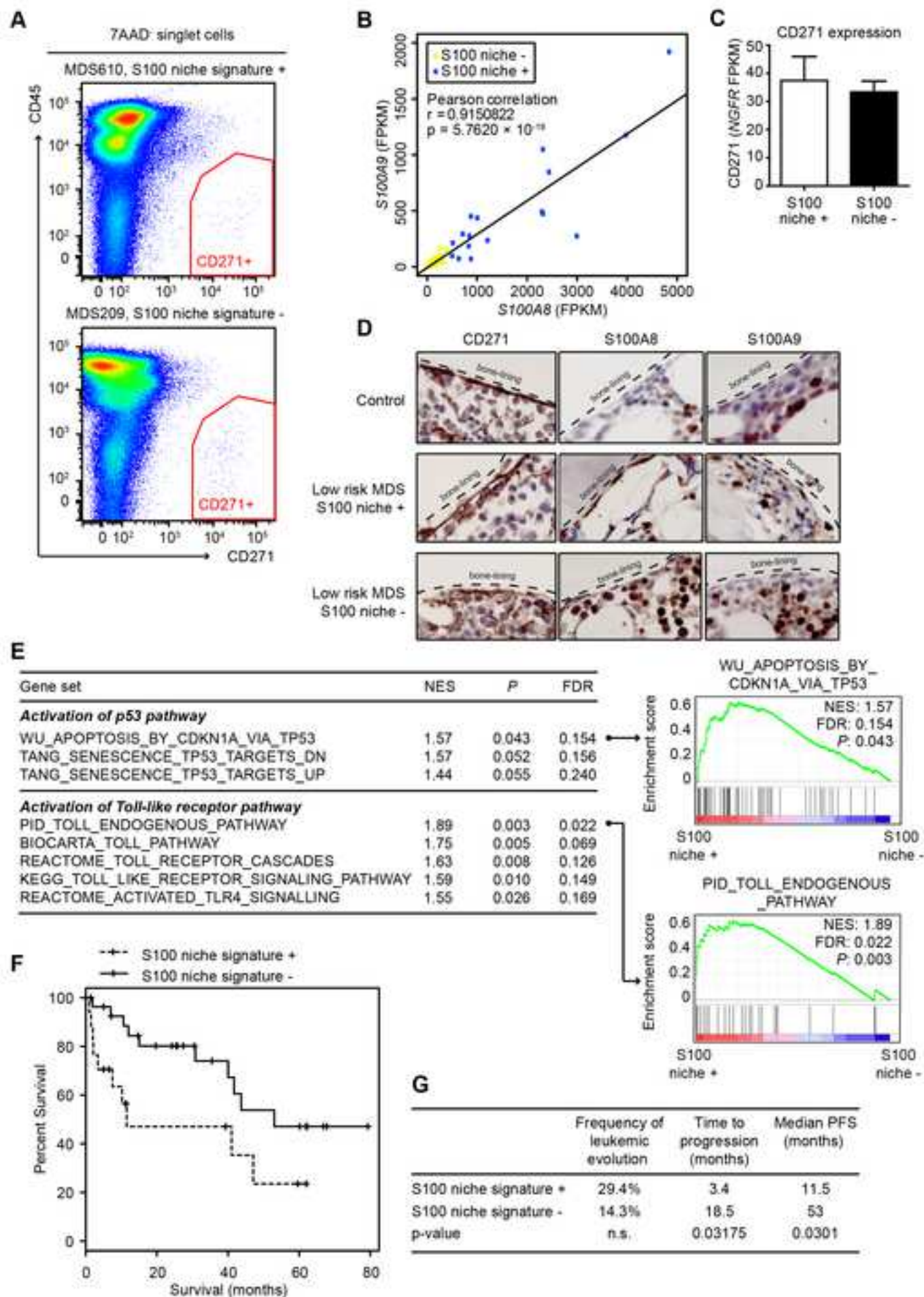












SUPPLEMENTAL DATA ITEMS

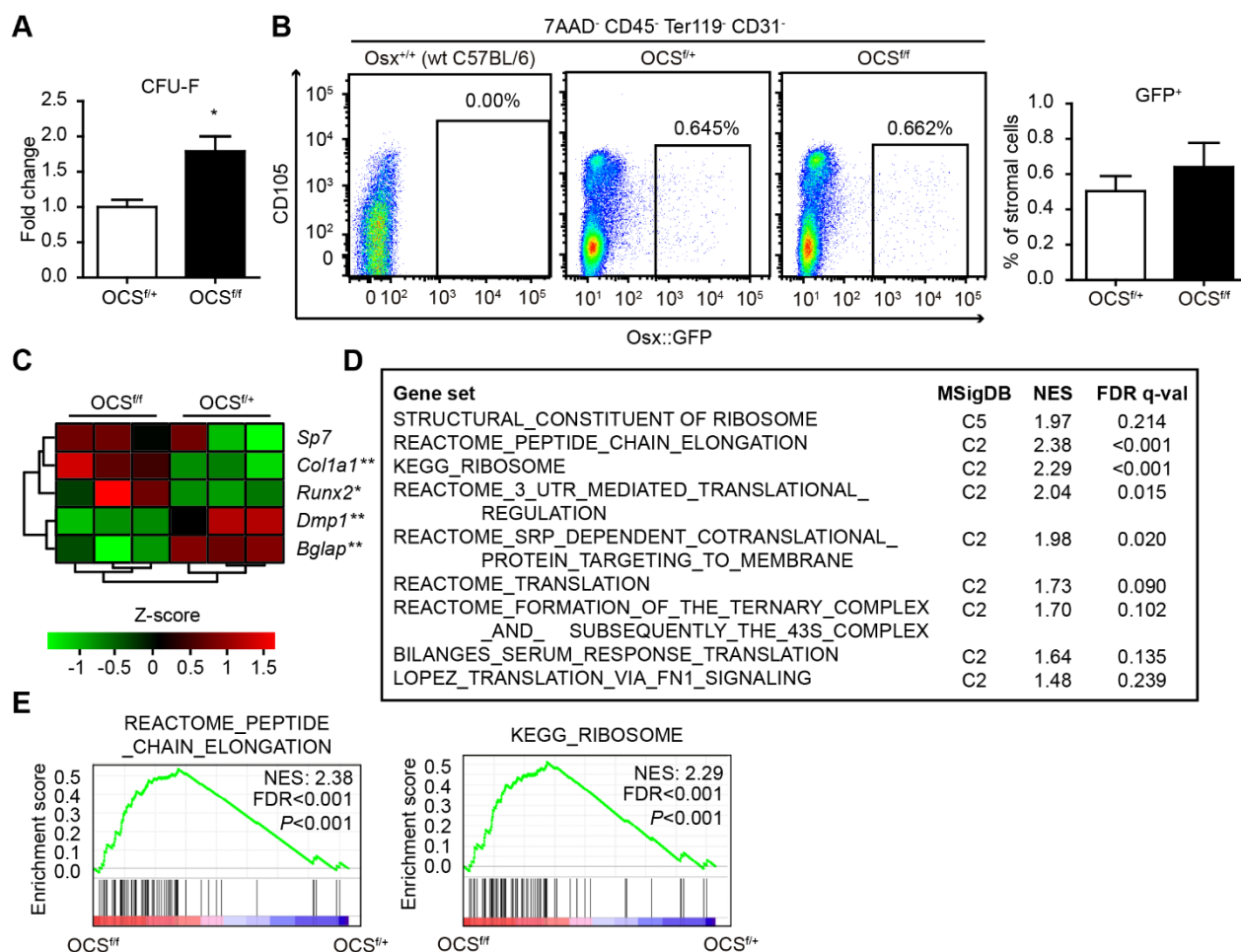


Figure S1. Related to Figure 1; Figure 4. Impairment of terminal osteogenic differentiation in OCS^{fl/fl} mice. (A) Increased CFU-F numbers ($n = 3$) with (B) unaltered frequency of Osx::GFP⁺ cells ($n = 4$) in OCS^{fl/fl} mice. (C) Depletion of transcripts defining terminal osteogenic differentiation (osteocalcin, *Bglap*) and dentin matrix acidic phosphoprotein 1 (*Dmp1*), critical for proper mineralization of bone, and enrichment of markers of bone progenitor cells or early osteoblasts (*Runx2* and *Col1a1*) in GFP⁺ cells from OCS^{fl/fl} mice. No statistically significant difference was observed in the expression of osterix (*Sp7*). (D) Significant (FDR<0.25) enrichment of ribosome and peptide chain elongation signatures in OCS^{fl/fl} GFP⁺ cells (GSEA) with (E) representative plots. * $P < 0.05$. ** $P < 0.01$. Data are mean \pm SEM.

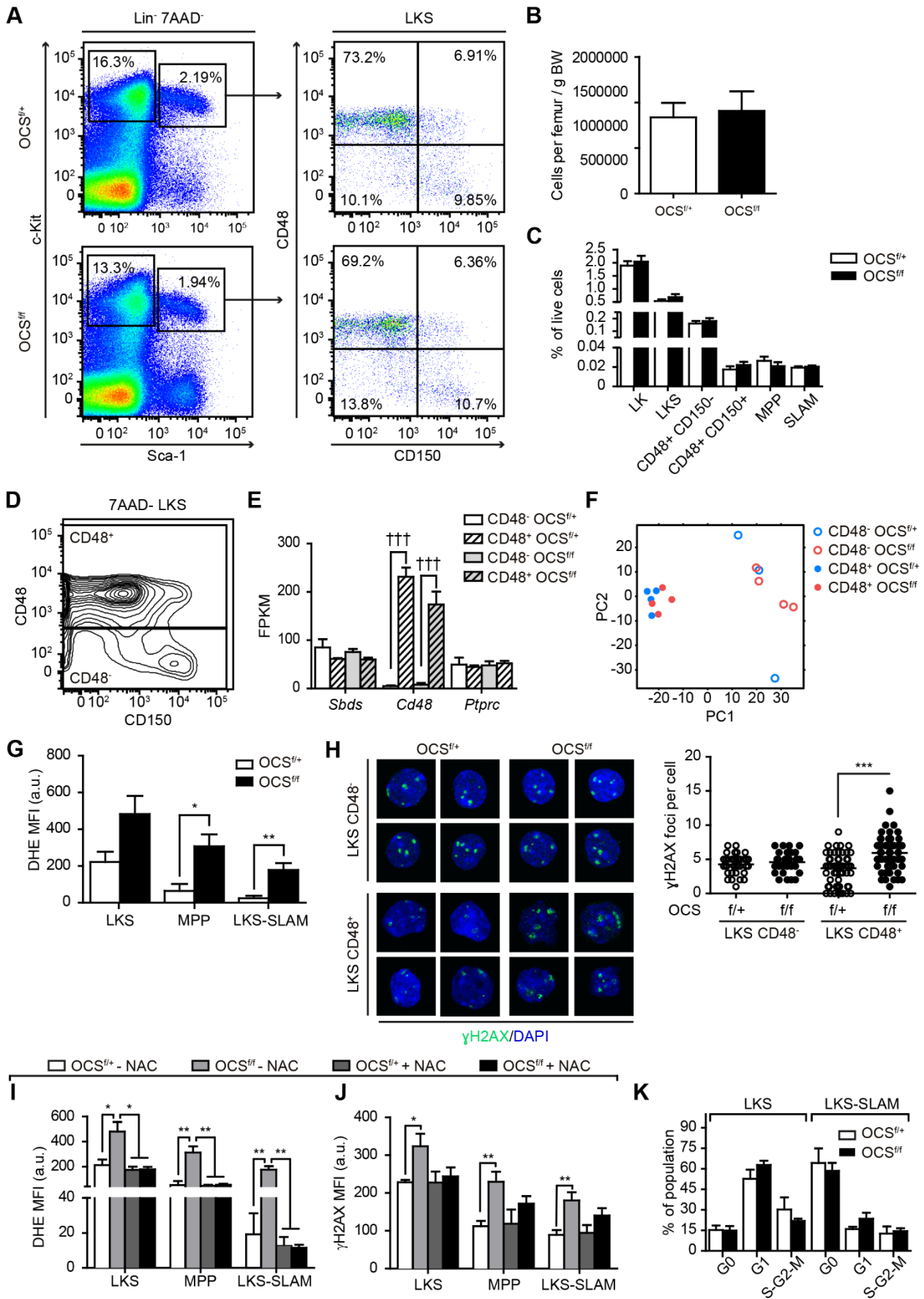


Figure S2. Related to Figure 2. Oxidative and genotoxic stress in HSPCs from OCS^{f/f} mice. (A-C) unaltered HSPC numbers in OCS^{f/f} mice: (A) representative FACS plots, (B) bone marrow cellularity and (C) subset frequency (OCS^{f/+}, $n = 8$ in A-B, $n = 7$ in C; OCS^{f/f}, $n = 7$). LK: Lin⁻ c-Kit⁺ Sca-1⁻ cells. LKS: Lin⁻ c-Kit⁺ Sca-1⁺ cells. MPP: multipotent progenitors, CD48⁻ CD150⁻ LKS cells. SLAM: CD48⁻ CD150⁺ LKS cells. (D) FACS isolation of CD48⁺ and CD48⁻ HSPC subsets for RNA-seq (OCS^{f/+} CD48⁻, $n = 3$; other groups, $n = 4$). (E) RNA-seq validation confirming CD48 and *Ptprc* (CD45) expression and the *Sbds*-proficient status of HSPCs from mutant mice. (F) Principal component analysis indicating global preservation of the transcriptome in HSPCs from OCS^{f/f} mice. (G) Superoxide radical accumulation in HSPCs from OCS^{f/f} mice as shown by DHE staining. (H) Increased number of γ H2AX foci in HSPCs from mutants ($n = 2$; pooled data). (I-J) NAC treatment attenuates oxidative (I) and (non-significantly) genotoxic stress (J) of OCS^{f/f} mice. NAC- controls were either treated with saline or not injected. (OCS^{f/+} + NAC, $n = 3$; OCS^{f/f} + NAC, $n = 3$; $n = 4$; other groups, $n = 5$). (K) Ki67 analysis of OCS mice indicating no change in the frequency of G0 HSPCs (OCS^{f/+}, $n = 3$; OCS^{f/f}, $n = 4$). * $P < 0.05$. ** $P < 0.01$. *** $P < 0.001$. †††FDR-adjusted $P < 0.001$. Data are mean \pm SEM.

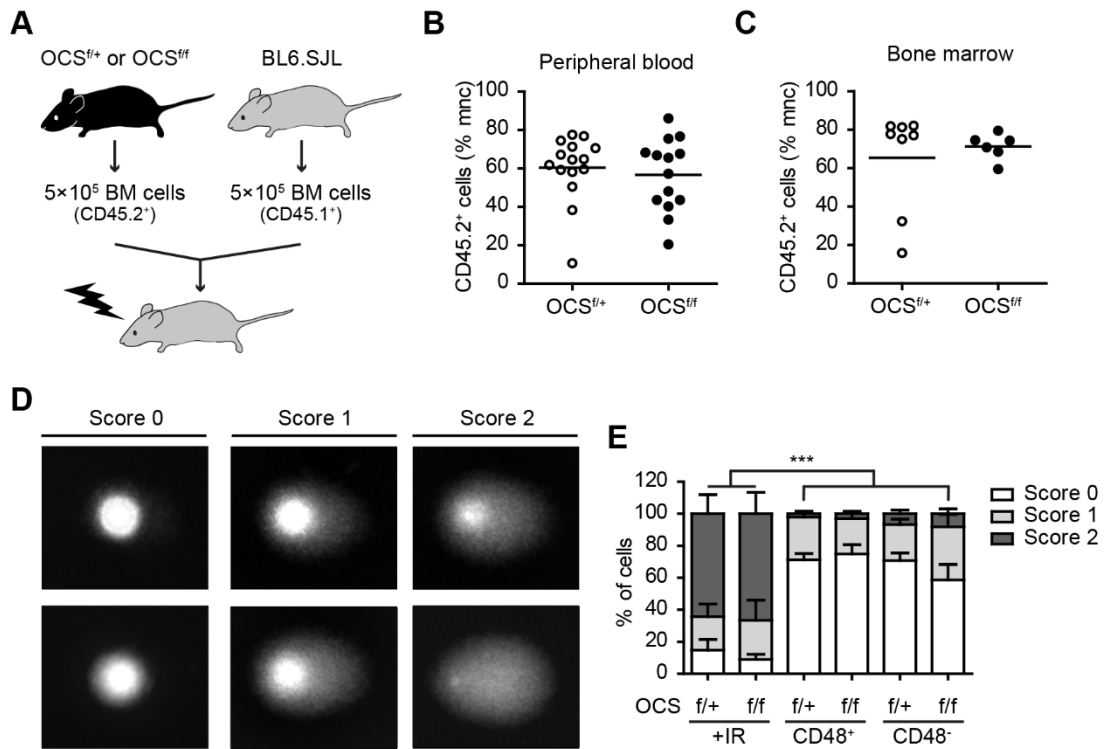


Figure S3. Related to Figure 2. Niche-induced DNA damage does not affect HSPC function. (A) Schematic representation of the competitive transplantation. BM: bone marrow. (B) Peripheral blood frequency of CD45.2⁺ cells 16 weeks after transplantation. (C) Bone marrow frequency of CD45.2⁺ cells (21-32 weeks after transplantation). Every circle represents one recipient mouse. (D) Manual scoring system applied to comet assay analysis. (E) Comet assay showing similar frequency of highly damaged HSPCs in OCS^{f/+} and OCS^{f/f} mice ($n = 5$). +IR: 8-10 Gy irradiated positive control (LK cells). *** $P < 0.001$. Data are mean \pm SEM.

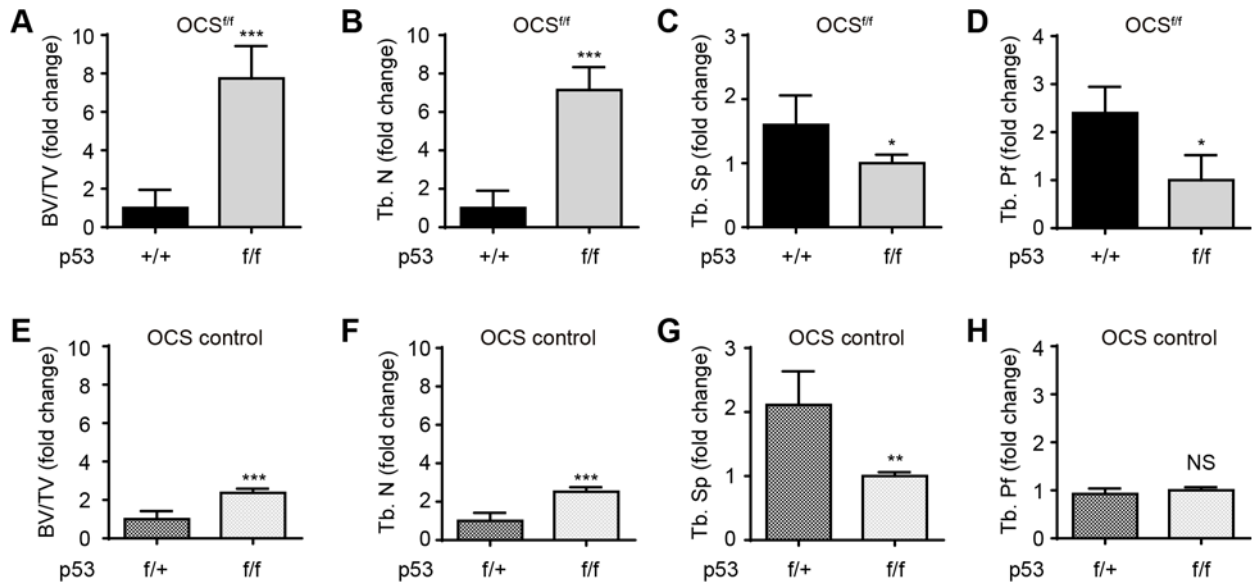


Figure S4. Related to Figure 3. Bone effects of *Trp53* ablation in OCS mutant and control mice. (A-D) Normalization of μ CT parameters in OCS^{f/f} p53^Δ mice shown as fold change (p53⁺, $n = 3$; p53^Δ, $n = 5$). (E-F) Modest increase in bone mass upon genetic deletion of p53 in OCS control mice, defined as *Osx*^{cre/+} *Sbds*^{f/+} or *Osx*^{cre/+} *Sbds*^{+/+} (p53^{f/+}, $n = 8$; p53^{f/f}, $n = 3$). * $P < 0.05$. ** $P < 0.01$. *** $P < 0.001$. Data are mean \pm SEM.

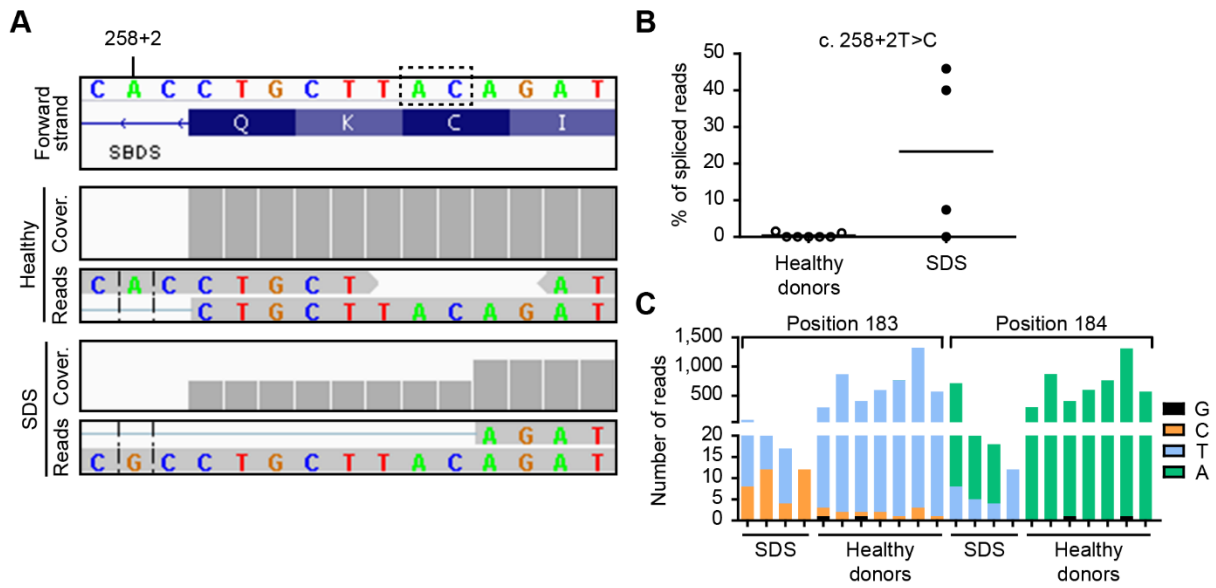


Figure S5. Related to Figure 4. *SBDS* mutations in mesenchymal cells from SDS patients. (A-B) Detection of 258+2 T>C mutation in SDS patients. (A) Representative IGV plot. Note that the coverage level after the cryptic site (dashed box) is reduced in SDS, indicating an 8-bp deletion. (B) Quantification of 258+2 T>C mutation as frequency of spliced reads with 8-bp deletion. Every circle represents a patient. (C) Nucleotide sequence in positions 183-184 from SDS patients and healthy donors.

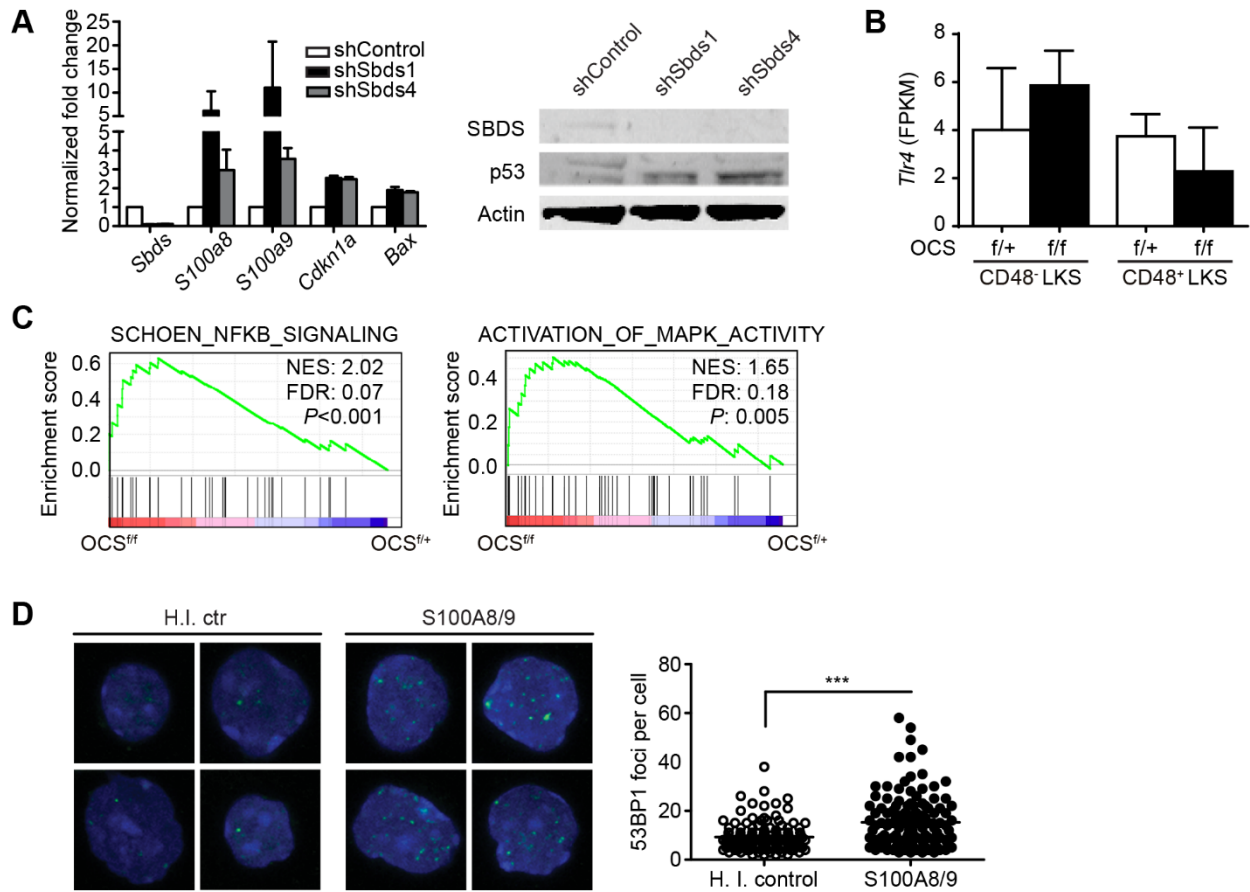


Figure S6. Related to Figure 2; Figure 5. A p53-S100A8/9-TLR axis induces DNA damage in HSPCs. (A) *Sbds*-knock down in OP9 cells induces expression of *S100a8*, *S100a9* and activation of p53 pathway. Left, expression analysis by qPCR (data normalized against shControl, $n = 3$). Right, representative Western Blot analysis showing p53 accumulation upon *Sbds*-knock down. (B, C) TLR4 expression and activation of NF- κ B and MAPK pathways in HSPCs from OCS^{f/f} mice (GSEA). NES: normalized enrichment score. (D) *Ex-vivo* treatment with S100A8/9 induces 53BP1 foci of DNA damage in murine HSPCs (LKS cells), Left, representative images. Right, cumulative dot plots ($n = 2$). *** $P < 0.001$. Data in bar graphs are mean \pm SEM.

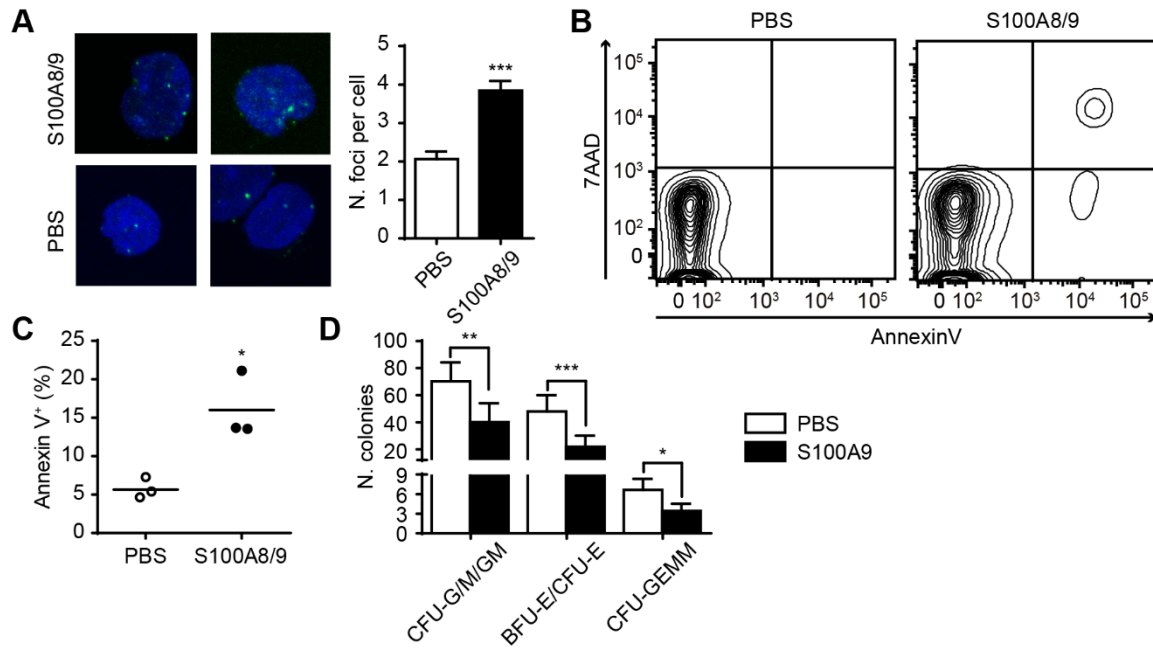


Figure S7. Related to Figure 5. S100A8/9 drives genomic stress in human HSPCs. (A-C) Treatment of human CD34⁺ HSPCs with recombinant S100A8/9. (A) Induction of γ H2AX foci ($n = 3$). (B-C) Increased frequency of apoptotic cells. (B) Representative plot. (C) Quantification ($n = 3$). (D) Reduced colony forming capacity of HSPCs as assessed by CFU-C assay ($n = 4$ independent experiments in triplicate). Data are mean \pm SEM. * $P < 0.05$. ** $P < 0.01$. *** $P < 0.001$.

Table S1. Related to Figure 2. Transcriptional profiling of OCS-derived HSPCs reveals dysregulation of signatures previously identified as predictive for leukemia evolution. Provided as an Excel file. Upregulation of G-protein-coupled receptors and cell adhesion-communication, and downregulation of mitochondrial oxidative phosphorylation, ribosome biogenesis, aminoacyl-tRNA synthetase activity, proteasomal degradation, citric acid cycle, cell cycle deregulation and hematopoietic stem cell programs. Normalized enrichment score (NES) and False Discovery Rate-adjusted q-value (FDR) are omitted when FDR > 0.25.

Table S2. Related to Figure 2. Stress and DNA damage dysregulation in the transcriptome of HSPCs from OCS^{f/f} mice.

ID	Description	CD48- LKS p-val	CD48+ LKS p-val
GO:0006310	DNA recombination	NS	4.68e-02
GO:0006950	response to stress	4.69e-05	1.31e-10
└ GO:0080134	regulation of response to stress	2.25e-03	9.78e-04
└ GO:0033554	cellular response to stress	5.53e-06	9.15e-05
└└ GO:0080135	regulation of cellular response to stress	2.82e-02	NS
└└ GO:0006974	cellular response to DNA damage stimulus	4.11e-03	1.96e-03
└└└ GO:0006281	DNA repair	3.86e-02	NS
└└└ GO:0006301	postreplication repair	NS	2.78e-02
REAC:5956042	Cell Cycle Checkpoints	1.27e-04	2.86e-04
└ REAC:5956049	Activation of ATR in response to replication stress	2.89e-02	4.10e-02
└ REAC:5956279	Gap-filling DNA repair synthesis and ligation in GG-NER	2.01e-02	NS
└ REAC:5956420	Gap-filling DNA repair synthesis and ligation in TC-NER	2.01e-02	NS

Genes with significantly different expression ($P < 0.05$) between OCS^{f/+} and OCS^{f/f} mice within the CD48⁻ or CD48⁺ populations were interrogated for GO and Reactome term enrichment using g-profiler. P-val: p-value. NS: not significant ($P \geq 0.05$).

Table S3. Related to Figure 2. Myc-related signatures depleted in OCS^{fl} HSPCs.

Gene set	Size	CD48- LKS		CD48+ LKS	
		NES	FDR q-val	NES	FDR q-val
DANG_MYC_TARGETS_UP	140	-2.3691	<0.0001	-2.3219	<0.0001
MENSSEN_MYC_TARGETS	52	-2.2803	<0.0001	-2.1716	<0.0001
YU_MYC_TARGETS_UP	40	-2.1026	<0.0001	-2.2127	<0.0001
ODONNELL_TARGETS_OF_MYC_AND_TFRC_DN	45	-1.9994	0.0004	-1.9883	0.0006
CAIRO_PML_TARGETS_BOUND_BY_MYC_UP	23	-1.9161	0.0015	-1.6278	0.0344
SCHUHMACHER_MYC_TARGETS_UP	80	-1.9014	0.0019	-2.2771	<0.0001
SCHLOSSER_MYC_TARGETS_REPRESSED_BY_SERUM	153	-1.8948	0.0021	-2.1315	0.0001
BENPORATH_MYC_TARGETS_WITH_EBOX	224	-1.8805	0.0025	-1.6005	0.0427
SANSOM_APC_TARGETS_REQUIRE_MYC	195	-1.8271	0.0049	-1.6294	0.0340
PID_MYC_ACTIVPATHWAY	77	-1.7735	0.0088	-1.7577	0.0107
MORI_EMU_MYC_LYMPHOMA_BY_ONSET_TIME_UP	102	-1.7638	0.0098	-1.9423	0.0012
SCHLOSSER_MYC_AND_SERUM_RESPONSE_SYNERGY	32	-1.7246	0.0142	-1.5919	0.0448
KIM_MYC_AMPLIFICATION_TARGETS_UP	192	-1.6787	0.0216	-1.8727	0.0027
DANG_REGULATED_BY_MYC_UP	69	-1.5696	0.0484	-1.7749	0.0091
COLLER_MYC_TARGETS_UP	25	-1.5656	0.0498	-2.0411	0.0003
ACOSTA_PROLIFERATION_INDEPENDENT_MYC_TARGETS_UP	77	-1.4380	0.1081	-1.4098	0.1455
SCHLOSSER_MYC_TARGETS_AND_SERUM_RESPONSE_DN	47	-1.4123	0.1260	-1.9374	0.0012
BILD_MYC_ONCOGENIC_SIGNATURE	193	-1.4101	0.1277	-1.3748	0.1735

Table S4. Related to Figure 4. Human normal donor and patient characteristics.

Sample ID	Disease status	Age	Sex
HD513	Healthy donor	40 y	M
HD723	Healthy donor	48 y	F
HD863	Healthy donor	42 y	M
HD237	Healthy donor	40 y	M
HD703	Healthy donor	39 y	M
HD066	Healthy donor	35 y	M
HD167	Healthy donor	48 y	M
SDS438	SDS patient ^a	9 y	M
SDS132	SDS patient ^a	14 y	M
SDS640	SDS patient ^a	4 y	M
SDS221	SDS patient ^a	18 y	M
MDS247	MDS patient ^b	59 y	M
MDS006	MDS patient ^b	62 y	F
MDS020	MDS patient ^b	71 y	F
MDS159	MDS patient ^b	74 y	F
MDS209	MDS patient ^b	78 y	F
MDS222	MDS patient ^b	66 y	F
MDS610	MDS patient ^b	64 y	F
MDS627	MDS patient ^b	80 y	M
MDS008	MDS patient ^b	67 y	F
DBA044	DBA patient	1 y	F
DBA087	DBA patient	4 mo	M
DBA563	DBA patient	4 y	F

^aAll SDS patients were genetically characterized by compound heterozygosity c.183_184TA>CT/c.258+2T>C. Patients did not receive G-CSF treatment and were not diagnosed with MDS or AML at the time of bone marrow sampling. All patients presented with pancreatic insufficiency (serum trypsinogen level <6 µg/L) and growth retardation (≤ 2 SD). All patients but SDS438 were neutropenic at sampling (absolute neutrophil counts, ANC < $1.5 \times 10^9/l$); SDS438 had ANC = $1.62 \times 10^9/l$).

^bSee Table S6 for further patient characteristics.

Table S5. Related to Figure S5. In vitro exposure of HSPCs to S100A8/9 activates transcriptional signatures related to TLR signaling and cellular stress/apoptosis.

Gene set	NES	p-val	FDR q-val
<i>Toll-like receptor signaling</i>			
BIOCARTA_TOLL_PATHWAY	1.60	0.014	0.404
REACTOME_TOLL_RECEPTOR_CASCADES	1.53	0.005	0.365
PID_TOLL_ENDOGENOUS_PATHWAY	1.49	0.043	0.380
KEGG_TOLL_LIKE_RECEPTOR_SIGNALING_PATHWAY	1.46	0.012	0.428
REACTOME_ACTIVATED_TLR4_SIGNALING	1.44	0.025	0.444
REACTOME_INNATE_IMMUNE_SYSTEM	1.56	0.0001	0.374
<i>Activation of p53 and apoptosis pathways</i>			
REACTOME_P53_DEPENDENT_G1_DNA_DAMAGE_RESPONSE	1.52	0.017	0.364
INGA_TP53_TARGETS	1.62	0.019	0.363
RASHI_RESPONSE_TO_IONIZING_RADIATION_1	1.68	0.005	0.326
DAZARD_UV_RESPONSE_CLUSTER_G2	1.69	0.006	0.314
AMUNDSON_GAMMA_RADIATION_RESISTANCE	1.71	0.009	0.316
KEGG_APOPTOSIS	1.74	0.001	0.260
KEGG_P53_SIGNALING_PATHWAY	1.78	0.001	0.217

Table S6. Related to Figure 7. MDS patient characteristics. Provided as an Excel file. All patients were treated with lenalidomide in the context of an ongoing prospective clinical trial (details in Experimental Procedures). Patient characteristics at study entry are listed. Progression free survival is calculated from date of study-entry. Hb, hemoglobin. PLT, platelets. WBC, white blood cells. ANC, absolute neutrophil count. *S100A8* and *S100A9* expression is obtained by RNA-sequencing data. P-values were calculated by Mann-Whitney (MW) test.

SUPPLEMENTAL EXPERIMENTAL PROCEDURES

Mice genotyping and sample collection

DNA was extracted from mouse toes with DirectPCR Lysis Reagent (Viagen Biotech). Genotyping and Cre-mediated recombination were verified on genomic DNA samples using the primers listed in the table below. Mouse bone marrow and bone fraction cells were isolated as previously described (Raaijmakers et al., 2010). Red blood cells (RBC) were lysed with ACK lysing buffer (Lonza) before surface markers staining. Peripheral blood was collected from the submandibular vein in K₂EDTA-coated microtainers (BD) and analyzed using a Vet ABC counter (Scil Animal Care).

Genotyping primers used in the study.

Target	Allele	Primer ID	Sequence	Amplicon size, bp
<i>Sbds</i>	Wild type	a	CCAGGGTCACGTTAATACAAACC	329
		b	TGAGTTTCAATCCTCAGCATCC	
	Floxed	a	CCAGGGTCACGTTAATACAAACC	450
		b	TGAGTTTCAATCCTCAGCATCC	
	Recombined	c	TAAAACAAAGCTGCGGTCAAGA	319
		d	ATCCTCAGCATCCCGAACA	
<i>Osx</i>	Wild type	e	CTCTTCATGAGGAGGACCCT	No band
		f	GCCAGGCAGGTGCCTGGACAT	
	Cre	e	CTCTTCATGAGGAGGACCCT	500
		f	GCCAGGCAGGTGCCTGGACAT	
<i>Trp53</i>	Wild type	10.1	GTTAAGGGGTATGAGGGACA	400
		10.2	GAAGACAGAAAAGGGGAGGG	
	Floxed	10.1	GTTAAGGGGTATGAGGGACA	600
		10.2	GAAGACAGAAAAGGGGAGGG	
	Recombined	1.1	CACAAAAACAGGTTAAACCCAG	612
		10.2	GAAGACAGAAAAGGGGAGGG	

Bone mineral density and 3-point bending test analysis

Cortical BMD was calculated from μ CT cortical data on the basis of a calibration scanning obtained using two phantoms with known density (0.25 g/cm³ and 0.75 g/cm³; Bruker MicroCT) under identical conditions as for the femurs. For the bending test, femurs were placed in a custom-modified Single Column Lloyd LRX System bending device (Lloyd Instruments) and analyzed as previously reported (van der Eerden et al., 2013) using CtAnalyzer software (Bruker MicroCT).

Goldner's Masson trichrome staining

Femurs were embedded in methylmetacrylate as indicated before (Derckx et al., 1998). Sections of 6 μ m were deacrylated, hydrated and stained accordingly to the previously described protocol (Gruber, 1992). Images of the metaphyseal area were captured with a Nikon Eclipse E400 system (Nikon) using a 20X objective lens. Data was analyzed using Image J software (<http://imagej.nih.gov/ij/>). Briefly, the bone surface was manually selected and the perimeter length calculated. Osteoblasts were manually identified based on staining and morphology. The frequency of osteoblasts was calculated as percentage of osteoblast area in the bone surface and as number of osteoblasts per mm of bone.

CFU-F assay

Primary bone fraction cells were resuspended in growth medium, consistent of α MEM, 20% FBS (Life Technologies), and Penicillin-Streptomycin solution (Life Technologies), and cultured under hypoxic conditions (5% O₂, 5% CO₂) in

24-well plates (seeding density: 6.5×10^4 cells/cm²). After 24h, the medium was changed to eliminate non-adherent cells. Colonies were stained after 7 days of culture. Briefly, medium was removed and cells were fixed 5' in methanol, stained in a 1:20 dilution of Giemsa staining (Merck Millipore) in distilled water and rinsed with tap water. Colonies were counted with an Olympus CK2 inverted microscope, using a 10X magnification.

Primary cell isolation and flow cytometry

All FACS antibodies incubations were performed in PBS+0.5%FCS for 20 min on ice. To identify hematopoietic stem and progenitor cells (HSPCs), bone marrow cells were first co-stained with a cocktail of biotin-labelled antibodies against the following lineage (Lin) markers: Gr1 (RB6-8C5), Mac1 (M1/70), Ter119 (TER-119), CD3e (145-2C11), CD4 (GK1.5), CD8 (53-6.7) and B220 (RA3-6B2) (all from BD Biosciences). After washing, cells were incubated with Pacific Orange-conjugated streptavidin (Life Technologies) and the following antibodies: Pacific Blue anti-Sca1 (D7), FITC or PE anti-CD48 (HM48-1), PE-Cy7 anti-CD150 (TC15-12F12.2) (all from Biolegend), APC anti-c-Kit (2B8, BD Biosciences).

To analyze differentiated cells and define chimerism, we used FITC anti-Gr1 (RB6-8C5), APC anti-Mac1 (M1/70), PE anti-B220 (RA3-6B2), APC-Cy7 anti-CD45.1 (A20), PE-Cy7 anti-CD45.2 (104), all from Biolegend. To identify stromal cells, bone fraction cell suspension was stained with the following antibodies: APC-Cy7 anti-CD45.2 (104), BV510 anti-Ter119 (TER-119), PE-Cy7 anti-CD105 (MJ7/18), PE anti-CD51 (RMV-7), Pacific Blue anti-Sca1 (D7) (all from Biolegend), PE-CF594 anti-CD31 (MEC 13.3, BD Biosciences).

For human mesenchymal cell isolation, bone marrow aspirates were diluted 1:25 with red blood cell lysis solution (NH₄Cl 0.155 M, KHCO₃ 0.01 M, EDTA-Na₂·2H₂O 0.1 M, pH 7.4) and incubated for 10 min at room temperature. Cells were collected by centrifugation and washed once with PBS+0.5%FBS. For FACS sorting, immunostaining was performed with the same protocol used for murine bone marrow, using PE CD271 (ME20.4) and PE-Cy7 CD45 (HI30) antibodies (Biolegend). CD271⁺ cells did not contain erythroid cells based on staining with BV421 CD235a (GA-R2, BD Biosciences).

Apoptosis was assayed with FITC Annexin V Apoptosis Detection Kit I (BD Biosciences) according to the recommendation of the manufacturer. Dead cells were excluded based on 7AAD staining.

The content of p53 in stromal cells was analyzed after cell surface antibody staining and cell permeabilization, obtained with Cytofix/Cytoperm Fixation/Permeabilization Solution Kit (BD Biosciences), by incubating cells with Alexa Fluor 647 anti-p53 (1C12) diluted in 1X Perm/Wash buffer (BD Biosciences).

γ H2AX levels were assessed in cells fixed and permeabilized with Cytofix/Cytoperm Fixation/Permeabilization Solution Kit (BD Biosciences) by incubating cells with Alexa Fluor 647 anti- γ H2AX (N1-431, BD Biosciences) diluted in 1X Perm/Wash buffer (BD Biosciences).

All FACS events were recorded using a BD LSR II Flow Cytometer and analyzed with FlowJo 7.6.5 software (Tree Star). Cells were sorted with a BD FACSAria III.

***SBDS* mutation analysis**

Mutations in *SBDS* were evaluated in the RNA sequencing data of SDS patients and healthy controls using the Integrative Genomics Viewer (IGV) (Robinson et al., 2011). The c.183_184TA>CT mutation was quantified by annotating the number of reads presenting each of the four different nucleotides for both the positions 183 and 184. Because of its intronic position, the c.258+2T>C mutation was assessed by quantifying the usage of the 251-252 cryptic donor site (Boocock et al., 2003). Specifically, we quantified the fraction of spliced reads with an 8-bp deletion (nucleotides 251-258) as an indication of the mutated genotype.

Mitochondrial membrane potential quantification

After staining cells for surface antigens, cells were washed in PBS+0.5%FBS and centrifuged. Cells were resuspended in PBS+0.5%FBS and tetramethylrhodamine methyl ester (TMRM, Life Technologies) was added from a 10 μ M stock solution in DMSO to a final non-quenching concentration of 100 nM. After incubation for 20 min at 37°C, cells were

washed with PBS+0.5%FBS and analyzed. Cells treated with 1 μ M p-trifluoromethoxy carbonyl cyanide phenyl hydrazone (FCCP) were used as positive control for membrane depolarization.

ROS detection

After surface antigen staining, cells washed in PBS+0.5%FBS and centrifuged. A stock solution of 2.5 μ g/ μ l 5-(and-6)-chloromethyl-2',7'-dichlorodihydrofluorescein diacetate acetyl ester (CM-H2DCFDA, Life Technologies) in DMSO was diluted with PBS+0.5%FBS to a final concentration of 3 μ g/ μ l. Cells were resuspended with the CM-H2DCFDA solution and stained for 20 min at 37°C, washed in PBS+0.5%FBS and analyzed.

For dihydroethidium (DHE) studies, the compound (Sigma Aldrich) was reconstituted to a 10mM solution in DMSO. After surface antigen staining and washing, cells were resuspended in 500 μ l of diluted DHE solution (1:10,000 in HBSS) and incubated at 37°C for 30 min, then washed in PBS+0.5%FBS and analyzed.

Cell cycle analysis

Mice labeled in vivo by BrdU were sacrificed and bone marrow cells were stained for surface antigen. BrdU staining was performed using the FITC BrdU Flow Kit (BD Biosciences) following the manufacturer's instructions.

For Ki67-based cell cycle analysis, cultured or freshly isolated cells were first stained for surface markers and then fixed and permeabilized with Cytotfix/Cytoperm Fixation/Permeabilization Solution Kit (BD Biosciences). After washing, cells were incubated cells with FITC anti-Ki67 (B56, BD Biosciences) diluted in 1X Perm/Wash buffer (BD Biosciences) for 20 min and then washed. Cells were resuspended in PBS+0.5%FBS and 7AAD was added to detect DNA.

Alkaline comet assay

HSPCs were resuspended in 0.7% low melting agarose (Sigma-Aldrich) in PBS at a concentration of 10⁵ cells/ml. 50 μ l of cell suspension were spread on CometSlides (Trevigen) and the agarose was allowed to solidify for 30 min at 4°C. Slides were incubated for 1 h at 4°C in lysis buffer (1% Triton-X100 freshly added to 2.5M NaCl, 100 mM EDTA, 10 mM Tris/pH10 solution) protected from light and placed in an electrophoresis tray. After 20 min incubation in alkaline solution (200mM NaOH, 1mM EDTA, freshly prepared), unwound DNA was run in the same solution for 30 min at 1 V/cm. After electrophoresis, slides were washed twice in distilled water for 5 min, fixated in 70% ethanol for 5 min and allowed to dry at 37°C. DNA was stained for 5 min in SYBR Gold (Life Technologies), washed in distilled water and allowed to dry in the dark. Images were captured with a Leica DMRXA fluorescent microscope (10X magnification). DNA damage severity was manually quantified according to the score system depicted in Figure S3D.

Bone marrow transplantation

For serial (competitive) transplantation studies, bone marrow cells from OCS and BL6.SJL mice were isolated and RBC-depleted as described above. BL6.SJL cells were mixed in a 1:1 ratio with cells from OCS^{f/+} or OCS^{f/f} mice. 9 week-old B6.SJL mice were lethally irradiated (8.5Gy) and transplanted with a total of 10⁶ bone marrow cells.

For transplantation in S100A9Tg mice, donor bone marrow cells were isolated from 12-week old BL6.SJL mice and transplanted into lethally irradiated (8.5Gy) C57BL/6 or S100A9Tg mice (F10 backcross in C57BL76). Each mouse received 2x10⁶ bone marrow cells by tail vein injection and was sacrificed one month after transplantation.

In all transplantation experiment, recipients received antibiotics in the drinking water for 2 weeks after transplantation.

S100A8/9 measurements

To quantify intracellular levels of S100A8/9 proteins, bone fraction cell suspensions were first stained for surface markers and next fixated and permeabilized with Cytotfix/Cytoperm Fixation/Permeabilization Solution Kit (BD Biosciences) according to the manufacturer's instructions. Cells were then resuspended in 1X Perm/Wash buffer (BD Biosciences) and incubated for 20 min with polyclonal rabbit antibodies against mouse S100A8 or S100A9 (Vogl et al., 2014). After washing, cells were incubated for 20 min with Pacific Orange-labelled goat anti-rabbit secondary antibody (Life Technologies) diluted in 1X Perm/Wash buffer, washed and resuspended in PBS+0.5%FBS and analyzed by FACS.

To analyze the concentration of S100A8/9 in the plasma, peripheral blood was collected in Microtainer PST tube (BD) and centrifuged to collect the plasma fraction. Samples were stored at -80°C until the moment of analysis. S100A8/9 was quantified by ELISA as previously described (Vogl et al., 2014).

Immunohistochemical staining of low-risk MDS and age-matched controls (biopsies obtained for disease staging from lymphoma patients without evidence of intramedullary localization) were performed on 5 µm bone marrow sections, which were deparaffinized in xylene and hydrated in a graded series of alcohol. Antigen retrieval was achieved by microwave treatment in citrate buffer (10mM pH 6.0) and blocking of the endogenous peroxidases was performed with 3% H₂O₂ in PBS. Sections were blocked using 10% normal human and goat serum (DAKO) in Teng-T solution followed by overnight incubation at 4°C with primary antibody anti-S100A8 and S100A9 (Vogl et al., 2014) diluted 1:500, CD271 (Sigma Aldrich) diluted 1:200, or normal rabbit immunoglobulin (DAKO) diluted accordingly. Immunoreactions were detected using biotinylated secondary antibody (goat anti-rabbit, 1:2000 dilution) with Vectastain ABC Elite Kit (Vector Laboratories) and 3,3'-diaminobenzidine tetrahydrochloride (Sigma Aldrich). For all stainings, nuclei were counterstained with haematoxylin (Vector Laboratories). Images of the stained tissue were acquired using a Leica DM5500B upright microscope with 40x lenses and LAS-AF image acquisition software.

Sbds-knockdown and expression analysis in OP9 cells

OP9 cells were grown in DMEM+10%FBS+1%PenStrep. *Sbds* RNA interference was achieved by lentiviral transduction. Briefly, short hairpin RNAs against *Sbds* (shSbds1:TRCN0000108586; and shSbds4:TRCN0000316346) and a commercial non-target control (shControl: SHC002 [SHC]), cloned in the pLKO.1 backbones, were selected from the Mission TRC shRNA library (Sigma-Aldrich). Lentiviral shRNAs were produced in HEK293T cells after cotransfection of shControl, shSbds1, or shSbds4 together with the packaging plasmids pSPAX2 and pMDG.2. OP9 cells were infected with lentivirus for 72 hours in the presence of 4 µg/mL polybrene and selected 72hours with 2 µg/mL puromycin.

RNA isolation, conversion to cDNA and qPCR were performed accordingly to previously described methods (Zambetti et al., 2015), using the SuperScript II Reverse Transcriptase (Thermo Fisher Scientific) for conversion to cDNA. For qPCR, expression levels were obtained using the ddCt method using GAPDH as internal control and shControl sample as calibrator. The following primers were used: *Sbds*-Fw: GCGCTTCGAAATCGCCTG; *Sbds*-Rv: TCTGGTCGTCGTCCCAAATG; *S100a8*-Fw: ATCACCATGCCCTCTACAAGAATG; *S100a8*-Rv: GTCCAATTCTCTGAACAAGTTTTTCG; *S100a9*-Fw: AAGCTGCATGAGAACAACCCA; *S100a9*-Rv: CCCAGAACAAAGGCCATTGA; *Cdkn1a*-Fw: CCTGGTGATGTCCGACCTG; *Cdkn1a*-Rv: CCATGAGCGCATCGCAATC; *Bax*-Fw: CCGGCGAATTGGAGATGAACT; *Bax*-Rv: CCAGCCCATGATGGTTCTGAT.

For protein analysis, cells were lysed in Carin lysis buffer (20 mM Tris-HCl pH 8.0, 138 mM NaCl, 10mM EDTA, 100 mM NaF, 1% NP-40, 10% glycerol, 2mM sodium vanadate) supplemented with 0.5 mM DTT and the protease inhibitor SigmaFast (Sigma Aldrich). 32 µg of protein per condition were denatured and separated on a Novex NuPage 4-12% Bis-Tris Gradient gel (Life Technologies) and transferred to Protran BA83 blotting paper (GE Healthcare Sciences). After blocking, membranes were incubated overnight at 4°C with the following primary antibodies: goat polyclonal anti-SBDS (Santa Cruz, S-15, 1:200); rabbit polyclonal anti- p53 (Leica, CM5, 1:2000). Beta-actin was used as a loading control (mouse monoclonal anti-beta-actin, clone AC-15, Sigma-Aldrich, 1:10,000 dilution). After washing, blots were incubated with the following secondary antibody: IRDye 800CW Donkey anti-Goat IgG (H + L), IRDye® 800CW Donkey anti-Rabbit IgG (H + L), and IRDye 800CW Donkey anti-mouse IgG (H + L) (all from Li-COR and diluted 1:10,000). After final washing steps, Western blots were scanned and processed using an Odyssey Infrared Imager (Li-COR Biosciences).

HSPCs in vitro culture, S100A8/A9 exposure and CFU-C assay

LKS and Lin⁻ c-Kit⁺ Sca-1⁻ cells were sorted from wild type C57BL/6 mice and cultured in a serum-free medium, with the following composition: X-Vivo 15 (Lonza), 1% detoxified BSA, 50 µM β-mercaptoethanol (Life Technologies), 1:100 GlutaMAX™ Supplement (Life Technologies), 20 ng/ml recombinant murine SCF (Peprotech), 100 ng/ml recombinant murine Flt3-Ligand (Peprotech), 1:100 penicillin-streptomycin mixture (Life Technologies). The medium was supplemented with recombinant murine S100A8/9, produced with the same methods described earlier (Vogl et al., 2006), at a final, clinically relevant concentration of 25-50 µg/ml, in the range of concentrations measured in the bone marrow supernatants of MDS patients (List, 2014). A heat-inactivated control was obtained by incubating S100A8/9 at 80°C for

30 min; the protein was cooled-down and next added to the HSPC medium with the same concentration and volume as S100A8/9. LKS and Lin⁻ c-Kit⁺ Sca-1⁻ cells were cultured in 96-well plates at a cell density of 2.5x10⁴ cells/well.

For human studies, cryopreserved CD34⁺ cells were used, which were isolated from cord blood obtained under informed consent by Ficoll gradient and MACS separation (Miltenyi Biotec). Thawed cells were resuspended in StemSpan SFEM II (STEMCELL Technologies) and recombinant human S100A8/9 was added (R&D systems) at a final concentration of 50 µg/ml. For the control medium, an equal volume of vehicle (PBS) was added. Cells were seeded in flat bottom 96 well-plates (5x10⁴ cells/well).

For both mouse and human studies, cells were harvested at 4h for γH2AX and cell cycle studies and at 24 h for apoptosis assay.

To assess the effect of S100A9 on HSPC function, CD34⁺ cord blood cells were resuspended in SFEM1 medium (Stemcell Technologies) containing SCF (50 ng/ml) and human recombinant S100A9 (2.5 µg/ml, ProSpec) or PBS control and seeded in 96-well plates (2x10⁴ cells/well). After one week of preconditioning (37°C, 5% CO₂), cells were pooled. 2,000 cells per condition were resuspended in 400 µl IMDM and transferred to 3.6 ml of MethoCult H84434 (Stemcell Technologies). Cells were plated in triplicate on 1 cm² petri-dishes (1 ml/dish) and incubated at 37°C/5% CO₂. Colonies were counted after 12-14 days.

SUPPLEMENTAL REFERENCES

Derkx, P., Nigg, A.L., Bosman, F.T., Birkenhager-Frenkel, D.H., Houtsmuller, A.B., Pols, H.A., and van Leeuwen, J.P. (1998). Immunolocalization and quantification of noncollagenous bone matrix proteins in methylmethacrylate-embedded adult human bone in combination with histomorphometry. *Bone* 22, 367-373.

Gruber, H.E. (1992). Adaptations of Goldner's Masson trichrome stain for the study of undecalcified plastic embedded bone. *Biotech Histochem* 67, 30-34.

List, A. (2014). Myeloid-Derived Suppressor Cells & Altered Innate Immunity in MDS Pathogenesis. <http://www.mds-foundation.org/wp-content/uploads/manual/ASH2014/6ListMDSF-ASH-253-12-5-14.pdf>

Robinson, J.T., Thorvaldsdottir, H., Winckler, W., Guttman, M., Lander, E.S., Getz, G., and Mesirov, J.P. (2011). Integrative genomics viewer. *Nat Biotechnol* 29, 24-26.

van der Eerden, B.C., Oei, L., Roschger, P., Fratzi-Zelman, N., Hoenderop, J.G., van Schoor, N.M., Pettersson-Kymmer, U., Schreuders-Koedam, M., Uitterlinden, A.G., Hofman, A., *et al.* (2013). TRPV4 deficiency causes sexual dimorphism in bone metabolism and osteoporotic fracture risk. *Bone* 57, 443-454.

Vogl, T., Eisenblatter, M., Voller, T., Zenker, S., Hermann, S., van Lent, P., Faust, A., Geyer, C., Petersen, B., Roebrock, K., *et al.* (2014). Alarmin S100A8/S100A9 as a biomarker for molecular imaging of local inflammatory activity. *Nat Commun* 5, 4593.

Vogl, T., Leukert, N., Barczyk, K., Strupat, K., and Roth, J. (2006). Biophysical characterization of S100A8 and S100A9 in the absence and presence of bivalent cations. *Biochim Biophys Acta* 1763, 1298-1306.